

# Reference Physics of CASCADE.04

H. Kumawat\*

*Nuclear Physics Division,  
BARC, Mumbai-400085, India*

(Dated: November 19, 2008)

## I. INTRODUCTION TO CASCADE.04

The CASCADE code realized the particle transport in three stages: 1) sampling of particle (ion) mean free path in the medium taking into account the energy loss of a charged particle and a possible decay of non-stable particles ( $\pi^0$ ,  $\pi^\pm$ ). All  $\pi^0$ -mesons are considered to decay into  $\gamma$ -quanta at the point of their creation. The ionization losses of  $\pi$  mesons, protons and light ions are calculated by Sternheimer's method [1, 2]. In the lower energy region Lindhard's approach [3] is used and a semi-phenomenological procedure [4] is applied for the heavy ions. 2) Simulation of the particle/nucleus interaction with a nucleus is considered along its path. In case of inelastic interaction the CASCADE code considers three stages of reactions for calculation: a) intranuclear cascade originally developed at Dubna: In this part of the calculation, primary particles can be re-scattered and they may produce secondary particles several times prior to absorption or escape from the target. Modeling of intra-nuclear cascades [5, 6, 7] is in general rather closer to the methods used in other transport codes. Cross-sections of the hadron-nucleus collisions are calculated based on the compilations of the experimental data [8, 9]. To calculate the nucleus-nucleus cross-sections we used analytical approximations with parameters defined in ref. [10]. Criteria of transition from intra-nuclear cascade to pre-equilibrium stage are the cutoff energy (binding energy above the Fermi energy), below which the particles are considered to be absorbed by the nucleus. Particles are traced down to this cutoff energy and then the second stage, pre-equilibrium starts, b) Pre-equilibrium stage: In this part of the reaction, relaxation of the nuclear excitation is treated according to the exciton model of the pre-equilibrium decay. The relaxation is calculated by the method based on the Blann's model [11, 12]. Proton, neutron, deuterium, tritium,  $^3\text{He}$  and  $^4\text{He}$  are considered as emitted particles in the pre-

---

\* author. Email address: harphool@barc.gov.in

equilibrium and in the subsequent equilibrium stage. Transition from pre-equilibrium to equilibrium state of the reaction occurs when the probability of nuclear transitions changing the number of excitons  $n$  with  $\Delta n = +2$  becomes equal to the probability of transitions in the opposite direction, with  $\Delta n = -2$ , c) Equilibrium stage: This part considers the particle evaporation/fission of the thermally equilibrated nucleus. In case of thick target simulation the last stage is to transport the low energy  $E_n \leq 10.5 \text{ MeV}$  neutrons down to thermal energies. The code uses 26-group constants [13] for neutron transport cross-sections below 10.5 MeV. The neutrons can moderate by numerous elastic collisions; can make fission in case of fissile/fertile materials and finally captured in  $(n, \gamma)$  reaction. It was assumed that cascade particle is stopped if its energy is less than the boundary energy  $E_b$  which equals to 2 MeV for  $\pi$ , 2 MeV for proton and, deuteron, 10 MeV for tritium and, 10 MeV/nucleon for all heavier nuclei. However, it is important to have a careful consideration of these low energy particles for biophysical problems, investigation of radiation damage to micro-electronic devices and some other applications where large radiation damage produced by low-energy particles are important[4]. Low energy  $\pi^-$  mesons are captured in a nucleus creating new intranuclear cascades. The algorithm is cyclic in nature and is reduced to several repetitions of all these possible operations.

## II. TIME DEPENDENT INTRA-NUCLEAR CASCADE MODEL

The intra-nuclear cascade stage is the fast stage ( $10^{-23} \text{ sec}$ ) of the particle interaction where knock out reaction, inelastic scattering, deep-inelastic scattering can take place. The interaction in INC model is treated as independent collision of the nucleons in the Fermi sea. In case of knock out reaction, one and/or two particles approx. are probable to be kicked out. Inelastic scattering may cause slight loss of energy to the incident particle/nuclei and leaving a small amount of energy to the residual/target nuclei. Deep inelastic scattering will cause several (order of ten) interactions inside the nuclei before escaping the target nuclei. During this process several particles/mesons will be emitted and a hot residual nuclei will be left behind which will decay/relax by emitting several particles/gammas in the pre-equilibrium and evaporation/fission/multifragmentation processes. Schematic diagram of the intra-nuclear cascade is shown in Figure 1. The basic principles of the intra-nuclear model used in the CASCADE.04 [14] are defined in ref. [5, 6, 7, 15]. The intra-nuclear model is used to simulate the reaction mechanism for particle-nucleus and nucleus-nucleus interactions. The particle-nucleus module does not incorporate the coalescence model but

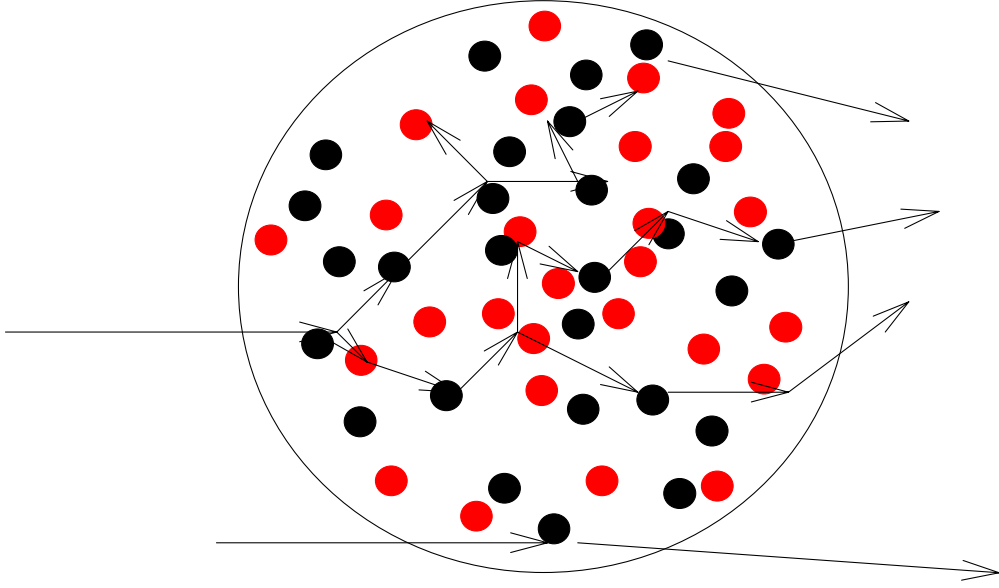


FIG. 1: Schematic diagram of the intra-nuclear cascade stage.

the nucleus-nucleus module does take into account as described in ref. [15].

The following condition should be fulfilled to apply the INC model which were noticed first time by Serber [16]:

1) de Broglie wave length should be shorter than inter-nucleon distance so that the interaction following classical trajectory remains valid.

$$\lambda \ll d$$

2) de Broglie wave length should be shorter than mean free path for the next collision

$$\lambda \ll \Lambda$$

3) mean free path should be shorter than target radius so that interference terms between collisions cancel out.

$$\Lambda < R$$

4) independent collisions between the nucleons inside target will be valid if

$$\left\{ \begin{array}{l} \Lambda > d \\ \Lambda/\beta c \text{ time between interactions} > \text{interaction time} \end{array} \right\}$$

In principle the following limitations are applicable to the INC model:

$$\left\{ \begin{array}{l} E(\text{incident}) \approx 50 \text{ MeV} \quad \text{for peripheral collisions} \\ E(\text{incident}) \approx 200 \text{ MeV} \quad \text{for deep inelastic collisions} \end{array} \right\}$$

The target nucleus is represented with continuous density distribution with Fermi gas momentum distribution. Fermi energy is calculated in local density approximation. The density dependent momentum/energy distribution is represented as

$$\left\{ \begin{array}{l} P_F(r) = (\frac{3\pi^2\rho(r)}{2})^{1/3} \\ E_F(r) = \hbar^2 \frac{(3\pi^2\rho(r))^{2/3}}{2m_N} \end{array} \right\}$$

The density distribution to calculate the Fermi momentum/energy is described by the single set of parameters as given below

$$\left\{ \begin{array}{l} \rho(r) = \frac{\rho_0}{1 + \exp(\frac{r-r_0}{a})} \\ \text{where} \quad r_0 = 1.07A^{1/3} fm \\ a = 0.545 fm \quad \text{For } A > 10 \\ \rho(r) = \rho_0 \exp(-\frac{r^2}{R^2}) \quad \text{For } A \leq 10 \end{array} \right\} \quad (1)$$

The curoff value of the radius (r) for the density distribution as well as for the impact parameter calculation is taken up to the value at which the density becomes 1% to that of a value at  $r_0$ .

The minimum internucleon distance inside the nucleus is assumed to 0.8fm to take into account the repulsive core (two nucleons can not come closer than 0.8fm). The nucleus must be centered at 0 in the configuration space, i. e.  $\Sigma_i r_i = 0$  and  $\Sigma_i p_i = 0$ . The projectile interacts with the nearest target nucleon met inside a cylinder of radius R as shown in Figure 2.

$$\left\{ \begin{array}{l} R = 1.3 fm + \lambda \\ \lambda \quad \text{is de-Broglie wavelength} \end{array} \right\}$$

The cascade evaluation is time dependent. The fastest cascade particle is simulated first. If time taken by the  $t_2$  particle is less then that will be considered as first cascade particle. The nucleon and pion potentials are defined as given below.

$$\left\{ \begin{array}{l} V \equiv V_N = E_F + \text{Binding energy} \\ V_\pi = 25 \text{MeV} \end{array} \right\}$$

Particles are emitted if permitted by the pauli exclusion principle and will be absorbed if the energy of the participant is less than Fermi energy+Binding energy (for neutron), and Fermi energy+Binding energy + Coulomb Energy (for protons).

Mean free path of the nucleons in the nucleus are sampled according to the local density and free N-N cross-sections. All parameters (cross-section and angles of the scattered nucleons/measosns) of the N-N and  $\pi$ -N interactions are adopted as described in ref. ???. The

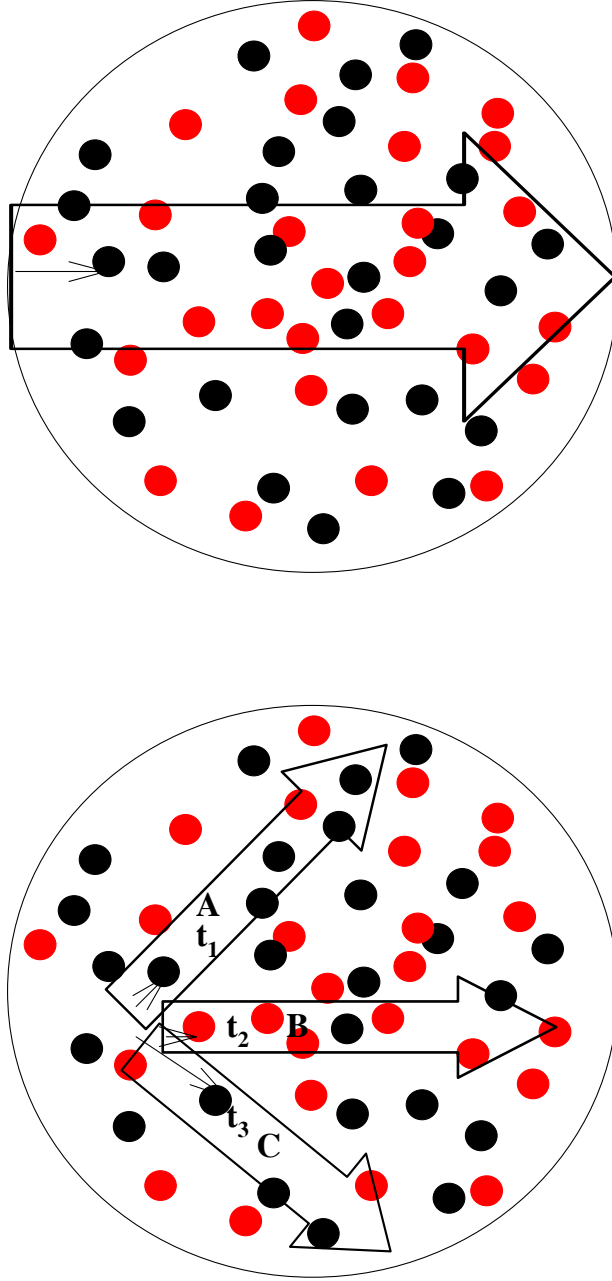


FIG. 3: Time dependent interaction of cascade particles inside the cylinders of radius  $R$  in different directions of motion of the particles.

cosine of the angle of emission in CM, in case of two particles in the final state, is calculated

with the help of uniform random number  $\xi$  as given below.

$$\left\{ \begin{array}{l} \cos(\theta) = 2\xi^{1/2} \left[ \sum_{n=0}^N a_n \xi^n + \left(1 - \sum_{n=0}^N a_n\right) \xi^{N+1} \right] - 1 \\ a_n = \sum_{k=0}^N a_{nk} E^k \\ N=3, M=3 \end{array} \right\} \quad (2)$$

where the coefficients  $a_{nk}$  at several energies (E) are the coefficients obtained after fitting then available experimental data. The coefficients for two body final state are for the following reactions.

$$\left\{ \begin{array}{ll} p + p = p + p & \text{Isotropic } E < 0.46 \text{ GeV} \\ p + p = p + p & 0.46 < E < 2.8 \text{ GeV} \\ p + p = p + p & 2.8 < E < 10.0 \text{ GeV} \\ p + n = p + n & E < 0.97 \text{ GeV} \\ \pi^+ + p = \pi^+ + p & E < 80.0 \text{ MeV} \\ \pi^+ + p = \pi^+ + p & 80 < E < 300.0 \text{ MeV} \\ \pi^+ + p = \pi^+ + p & 0.3 < E < 1.0 \text{ GeV} \\ \pi^+ + p = \pi^+ + p & 1.0 < E < 2.4 \text{ GeV} \\ \pi^- + p = \pi^- + p & E < 80.0 \text{ MeV} \\ \pi^- + p = \pi^- + p & 80 < E < 300.0 \text{ MeV} \\ \pi^- + p = \pi^- + p & 0.3 < E < 1.0 \text{ GeV} \\ \pi^- + p = \pi^- + p & 1.0 < E < 2.4 \text{ GeV} \\ \pi^- + p = \pi^0 + n & E < 80.0 \text{ MeV} \\ \pi^- + p = \pi^0 + n & 80 < E < 300.0 \text{ MeV} \end{array} \right\}$$

The angular distribution above the upper limit of the above reactions are defined for the given momentum (P) as

$$\left\{ \begin{array}{l} \text{For } p + p \text{ or } n = p + p \text{ or } n \\ \cos(\theta) = 1 + \frac{2(\log(1+\xi(\exp(-8.7P)-1)))}{8.7P} \\ \text{For } \pi + p \text{ or } n = \pi + p \text{ or } n \\ \cos(\theta) = 1 + \frac{2(\log(1+\xi(\exp(-7.5P)-1)))}{7.5P} \end{array} \right\}$$

The coefficients for many body final state are for the following reactions. The separate

coefficients are given for nucleons and pions angular distribution.

$$\left\{ \begin{array}{ll} N + N = 2N + \pi & \text{For nucleons} \\ N + N = 2N + \pi & \text{For pions} \\ N + N = 2N + n\pi & n > 1; \text{For nucleons} \\ N + N = 2N + n\pi & n > 1; \text{For pions} \\ \pi + N = N + 2\pi & \text{For nucleons} \\ \pi + N = N + 2\pi & \text{For pions} \\ \pi + N = N + n\pi & n > 2; \text{For nucleons} \\ \pi + N = N + n\pi & n > 2; \text{For pions} \end{array} \right\}$$

Azimuthal angle is assumed to be isotropic. Momentum distribution of the secondary particles is simulated as given below

$$\left\{ \begin{array}{l} p = p_{max} \xi^{1/2} \left[ \sum_{n=0}^3 b_n \xi^n + \left(1 - \sum_{n=0}^N b_n\right) \xi^{N+1} \right] - 1 \\ p_{max} = \sum_{k=0}^{M-1} c_k E^k \\ N=3, M=3 \end{array} \quad b_n = \sum_{k=0}^M b_{nk} E^k \right\} \quad (3)$$

The coefficients are defined for all the many body final state reactions. Two body final state calculations are done by usual kinematics taking into account the energy/momentum conservation after simulation of the angle of secondary particles.

### A. Nucleon-Nucleus and pion-nucleus cross-sections

Hadron/pion nucleus cross-section are adopted in CASCADE.04 from ref. [9]. These data base are generated with minimum  $\chi^2$  values from the experimental data [8]. The tabulated inelastic and elastic data are given from 10MeV up to 10TeV for neutron, 1MeV up to 10TeV for proton and 1MeV up to 10TeV for  $\pi^+$  and  $\pi^-$ . The energy steps are 1-2MeV at below 50MeV and it increases with increase in energy, where the variation of the cross-sections becomes smooth. The list of energies and elements are given below for which the data are tabulated in the CASCADE.04. Quadratic interpolation is adopted to obtain the cross-section for a particular mass and energy. One example of the neutron-nucleus for Deuteron, iron and lead are shown in 4. More details about these cross-sections can be found in [8, 9]

These cross-sections are never used in the thin target calculations. The probabilities distributions (neutral and charged particle double differential production and residual nuclei productions) generated by the code are used to get the cross-section by multiplying these

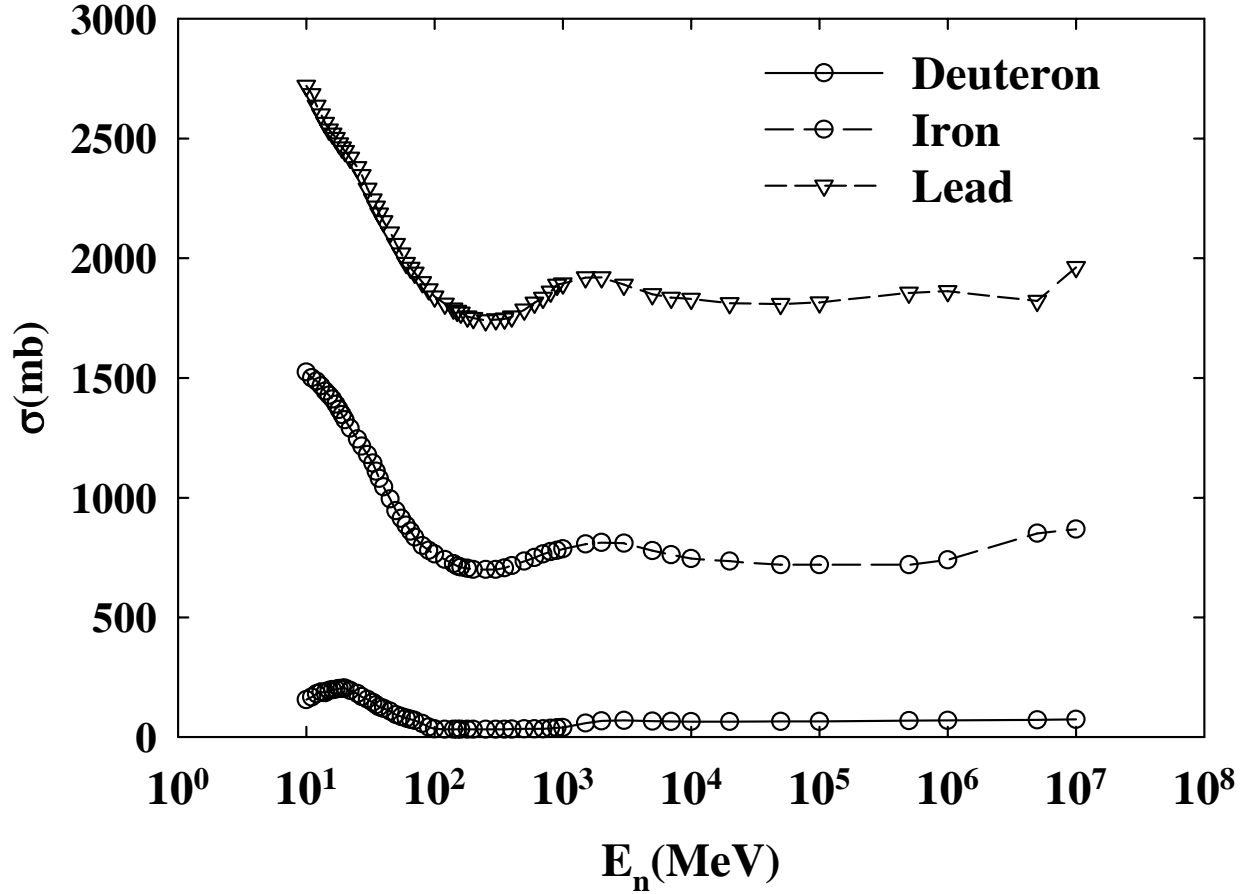


FIG. 4: Energy/mass dependency of inelastic cross-sections for n+Deuteron, Iron and lead as adopted in CASCADE.04.

distributions with the inelastic/reaction cross-sections given in Tables II and I. Thus these cross-sections don't affect the model calculations. In case of thick target, after selecting the nuclei to be interacted, these cross-sections are used in the early stage of the calculations to decide the inelastic or elastic reaction mechanism. Thus it is important to have right values of the cross-sections to transport the particles in the matter.

### B. Nucleus-Nucleus cross-sections

The cross-sections of inelastic and elastic interactions of nuclei are necessary for solution of various theoretical and applied problems, in particular, for modelling transport of particle and ion beams in media for a designing of electronuclear systems, radiation shielding, estimations of radiation damage to microelectronic devices, radiobiological effects from clinical exposures and knowledge of beam interactions is important to evaluate the effects on

TABLE I: List of elements for which neutron, proton and pion nucleus cross-sections are included in CASCADE.04

Neutron and proton		$\pi^\pm$	
H	1.0	He	4.0
D	2.0	Be	9.01
He	4.0	C	12.0
Li	6.90	N	14.0
Be	9.01	O	16.0
C	12.00	Na	23.0
N	14.00	Al	26.98
O	16.00	S	32.08
Na	23.00	Ca	40.08
Al	26.98	Ti	47.90
S	32.00	Fe	55.85
Ca	40.08	Cu	63.55
Ti	47.90	Br	79.90
Fe	55.85	Mo	95.94
Cu	63.50	Cd	112.40
Br	79.90	Sn	118.69
Mo	95.94	Ba	137.34
Cd	112.40	W	183.85
Sn	118.7	Pb	207.19
Ba	137.34	U	238.03
W	183.85	Cf	
Pb	207.19		
U	238.03		
Cf	251.0		

human and animal tissue. Such cross-sections are especially important for the calculation of cosmic ray interactions with details of satellites where heavy nuclei of the iron group give a large contribution. To evaluate the dose of exposures one need reliable transport code and that needs accurate input data. One of these input data is total (inelastic and elastic)

TABLE II: List of energies for which neutron proton and pion nucleus cross-sections are included in CASCADE.04

Neutron	Proton	energy(MeV)
10	1	1
11	2	3
12	3	5
13	5	10
14	7	15
15	8	20
16	9	30
17	10	40
18	11	50
19	12	60
20	13	70
22	14	80
25	15	90
27	16	100
30	17	110
33	18	120
35	19	130
37	20	140
40	22	150
45	25	160
50	27	170
55	30	180
60	33	190
65	35	200
70	37	220
80	40	240
90	45	250
100	50	260
120	55	280
140	60	300
150	65	350
160	70	400
180	80	450
200	90	500
250	100	550

cross-section.

Many theoretical studies [17, 18, 19, 20, 21, 22] in this regard are available. However, experimental information about cross-sections is very poor[8]. Presently, the only way to get necessary data is an interpolation and extrapolation of the known experimental points by means of some analytical expressions with fitted parameters prompted by theoretical models. Now there are several such approximations in rather narrow energy and mass number intervals. The most universal and simple, applicable for energies higher the coulomb barrier and for various nucleus pairs is considered in [8, 23]. Expressions approximating the experimental integral cross-sections for elastic and inelastic interactions of light and heavy nuclei at the energies up to several GeV/nucleon are given below. The calculated cross-sections are in the limit of experimental errors.

The formula for the inelastic cross-section given in [17] is given below where constant C must be defined by the help of the experimental cross-section.

$$\sigma \frac{E}{A_p} = 38.011(1 - \frac{B}{E_c})(A_p^{1/3} + A_t^{1/3}) + 1.85A_{pt} - C(\frac{E}{A_p})^2 \quad (4)$$

Here E is the projectile nucleus energy in laboratory frame,  $E_c = A_{pt} \times E / A_p$  is CMS nucleus energy,  $A_{pt} = A_p A_t / (A_p + A_t)$ ,  $A_p$  and  $A_t$  are the projectile and target nuclei mass numbers, B is the Coulomb barrier. This approximation is based on a model combining central (with small impact parameters) and peripheral collisions. The parameter C characterizing the transparency of the nucleus periphery is a smooth function of the energy  $E/A_p = E_o / A_t$ , where  $E_o$  is the energy in the opposite reference frame. This function is defined by comparison with all known experimental data[8].

The precision of approximation of inelastic cross-section  $\sigma_{in}$  increases if  $C(E/A_p)$  is chosen separately for deuteron  $C_d$  and for more heavy nuclei  $C_h$ . Experimental information on the elastic cross-sections  $\sigma_{el}$  is much less, so  $C_{el}$  can be defined at once for all nuclei without separation of the light and heavy ones. We see that the cross-section eq. 4 is symmetrical with respect to laboratory and opposite coordinate systems.

One would try to improve the approximation and distinguish the cross-sections of isotopes [8, 23] by introducing the additional term  $\alpha(1 - Z_p/A_p - Z_t/A_t)$  into eq. 4. However, the coefficient  $\alpha$  is defined with too big error and Table III is calculated without this term.

In the most practical important cases the low boundary of approximation (1)  $E_b = B(1 + A_p/A_t)$  is less than the thresholds at which the ions are considered as stopped ones due to the fast increasing influence of ionization processes and we do not need the cross-sections at  $E \leq E_b$ . However, for heavy projectiles which we encounter, for example, in

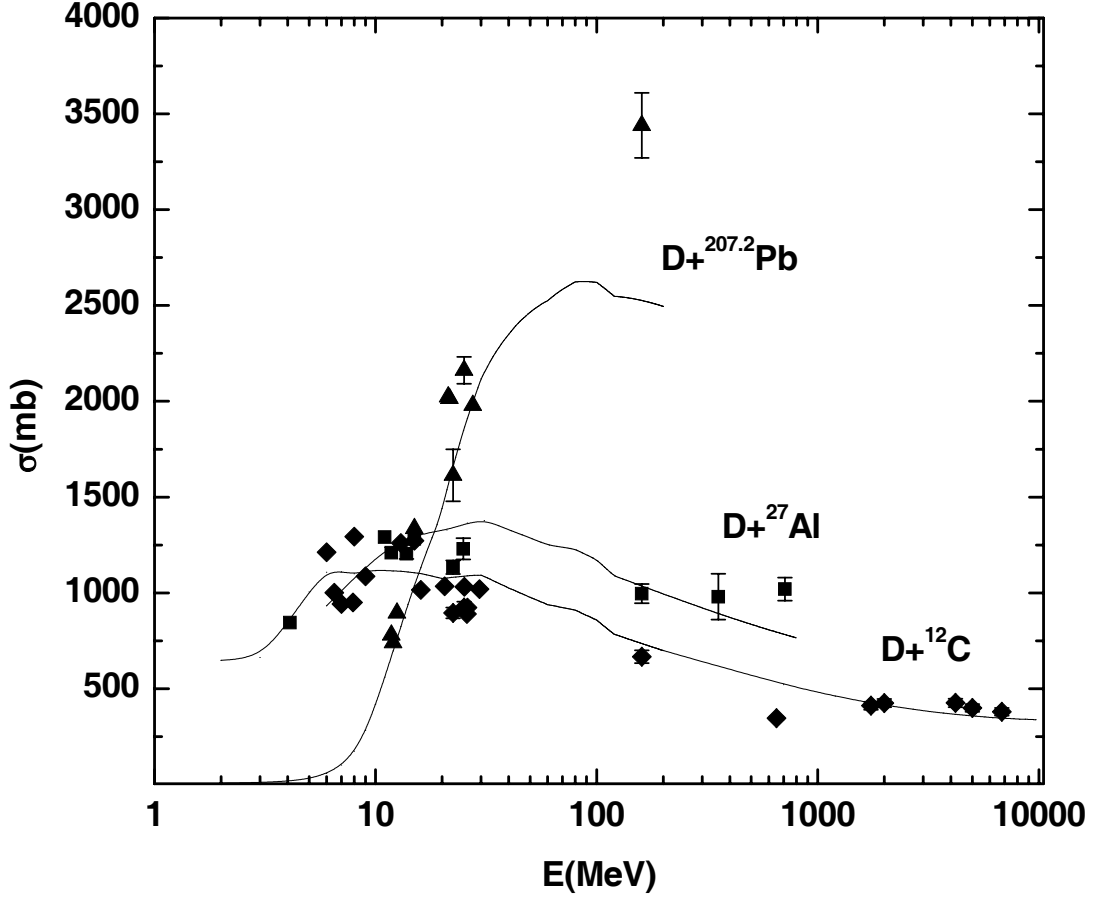


FIG. 5: Energy/mass dependency of inelastic cross-sections. Deuteron interaction with carbon, aluminum, and lead. Experimental points from compilation [8]. Lines represent the calculated/adopted values in CASCADE.04.

collisions of the iron component of cosmic rays with matter or in the experiments with the collisions of uranium nuclei the boundary  $E_b$  is large:  $E_b \gg B$ . (For  $\text{Fe} + \text{Fe}$  and  $\text{U} + \text{U}$  interactions  $B \approx 90$  and  $700$  MeV). In these cases one must use the approximation taking into account quantum effects in the vicinity of the coulomb barrier  $B$ . We shall use for that the expression obtained in refs. [24, 25].

$$\sigma = \frac{\alpha}{E} \ln\left(\frac{E_c - B}{\beta}\right) \quad (5)$$

Here  $\alpha$  is a normalization coefficient defined by sewing together with eq. 4 at some energy closer to  $B$  (we use  $E_c = B/0.61$ ),  $\beta = 1.095$  is a fitted constant. Approximation becomes somewhat more exact if the energy dependence of nuclear radius  $R_0(E) = R_0(1 - 0.021E/A_p)$  is introduced where  $R_0 = 2.1, 1.71, 1.47$  for deuteron,  $\alpha$ -particle and all other nuclei. The low

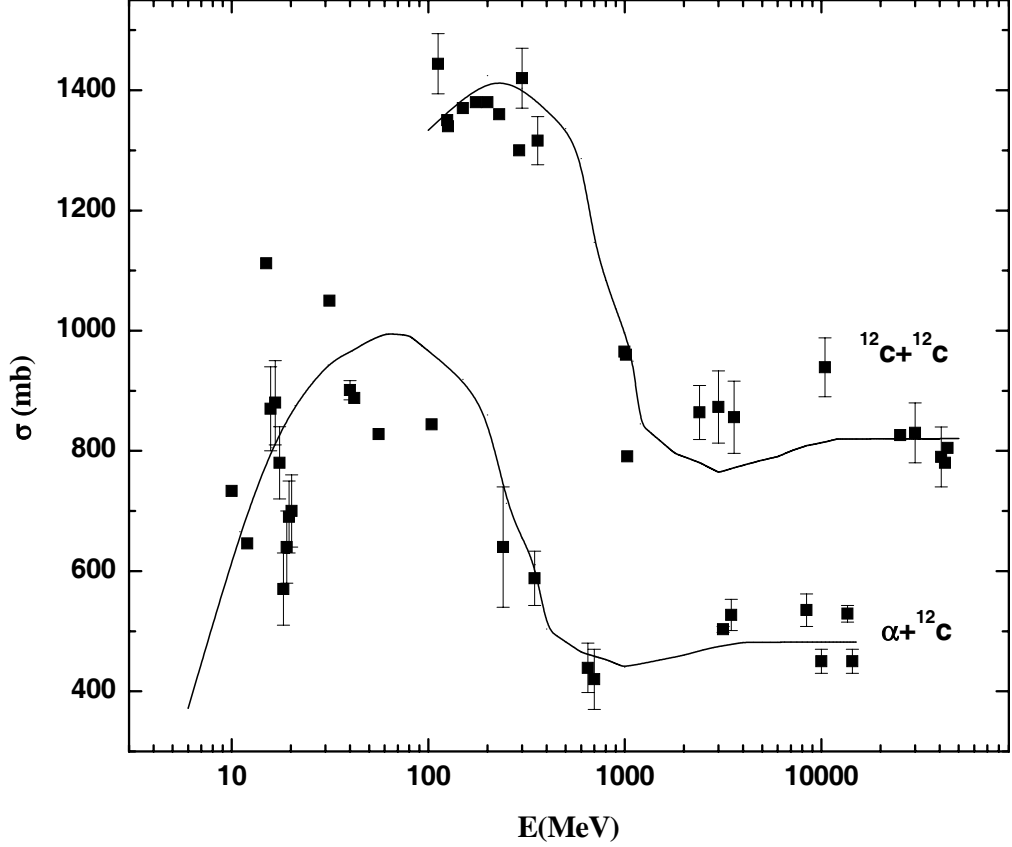


FIG. 6: Comparison of experimental and calculated inelastic cross-sections of  ${}^4\text{He}+{}^{12}\text{C}$  and  ${}^{12}\text{C}+{}^{12}\text{C}$  interaction. Experimental points from compilation [8]. Lines represent the calculated/adopted values in CASCADE.04.

boundary for this approximation is defined by the condition  $d\sigma/dE=0$  (at the lower energies  $\sigma$ , in spite of the experiment, is increasing due to  $T_c$  in the denominator).

Figures 6 and 5 illustrate the precision of the considered approximation for light nuclei. There are only few separate experimental data for heavy nuclei. The comparison with the calculated data is shown in Table IV. Taking into account the big experimental errors one can say that the calculated data are in the limit of errors. In table V elastic cross-sections are compared. In average, uncertainties of experimental data and calculated values are much larger than for  $\sigma_{in}$  in this case. In all cases when there are from two experimental values at the same energy, we present the averaged value: [24, 25].

$$\sigma \pm \sigma = \frac{\sigma_1 \Delta \sigma_2^2 + \sigma_2 \Delta \sigma_1^2}{\Delta \sigma_1^2 + \Delta \sigma_2^2} \pm \frac{\Delta \sigma_1 \Delta \sigma_2}{\sqrt{\Delta \sigma_1^2 + \Delta \sigma_2^2}} \quad (6)$$

TABLE III: Energy dependency of the function  $C(\log(E/A_p, \text{ MeV}))$ 

$\log(E/A_p)$	$C_d$	$C_h$	$C_{el}$	$\log(E/A_p)$	$C_d$	$C_h$	$C_{el}$
0	-.791	0.12	0.80	2.301	1.091	2.1	2.55
0.477	-.582	0.14	0.85	2.398	1.196	2.15	2.70
0.602	-.172	0.165	0.89	2.477	1.279	2.2	2.80
0.699	-.021	0.18	0.94	2.602	1.405	2.183	2.95
0.778	-.888	0.2	0.97	2.699	1.498	2.15	3.05
0.845	-.789	0.21	1.00	2.778	1.569	2.13	3.10
0.903	-.707	0.22	1.02	2.845	1.627	2.1	3.12
0.954	-.625	0.24	1.06	2.903	1.675	2.08	3.05
1	-.556	0.26	1.09	2.954	1.715	2.06	3.01
1.176	-.501	0.29	1.12	3.0	1.749	2.05	2.90
1.301	-.278	0.36	1.19	3.176	1.869	2.0	2.85
1.398	-.123	0.45	1.29	3.301	1.939	1.98	2.82
1.477	-.003	0.54	1.39	3.398	1.984	1.98	2.82
1.602	0.096	0.64	1.47	3.477	2.016	1.98	2.80
1.699	0.252	0.8	1.61	3.602	2.054	1.98	2.79
1.778	0.472	1.2	1.85	3.699	2.072	1.98	2.78
1.845	0.554	1.35	1.94	3.778	2.081	1.98	2.77
1.903	0.625	1.5	2.03	3.845	2.083	1.98	2.76
1.954	0.687	1.6	2.10	3.903	2.084	1.98	2.80
2 0	.743	1.7	2.16	3.954	2.085	1.98	2.82
2.176	0.949	1.95	2.40	4.0	.085	1.98	2.83

### III. EXCITON MODEL

The exciton model considers particle-hole configuration of the excited nuclei left after intra-nuclear cascade stage. All possible nuclear transitions changing the number of excitons  $n = (p+h)$ , here  $p$  denotes particles and  $h$  denotes holes, with  $\Delta n = \pm 2$  and  $0$  are considered, though some of the models does not consider  $-2$  transition (never come back approach). The possible multiple emissions of  $n$ ,  $p$ ,  $d$ ,  $t$ ,  ${}^3\text{He}$ , and  ${}^4\text{He}$  are taken into account till the residual nuclei gets equilibrium stage. The state of the equilibrium is obtained when all the three transition probabilities are equi-probable.

TABLE IV: Experimental and calculated (adopted in CASCADE.04 ) inelastic nucleus-nucleus interaction cross-sections

Nuclei	E (MeV)	$\sigma_{in}(\text{experiment})$	$\sigma_{in}(\text{calculation})$
$^{12}\text{C} + ^{54}\text{Fe}$	360	$2195 \pm 140$	2344
	996	$1795 \pm 70$	1925
$^{12}\text{C} + ^{55.8}\text{Fe}$	2400	$1643 \pm 46$	1638
	3000	$1596 \pm 46$	1618
	3600	$1588 \pm 46$	1631
$^{12}\text{C} + ^{56}\text{Fe}$	360	$2296 \pm 160$	2344
	996	$1838 \pm 70$	1925
$^{12}\text{C} + ^{57}\text{Fe}$	996	$1797 \pm 70$	1941
$^{20}\text{Ne} + ^{27}\text{Al}$	600	$2146 \pm 88$	2161
	2000	$1446 \pm 120$	1526
	6000	$1328 \pm 120$	1438
	64000	$1520 \pm 70$	1508
$^{20}\text{Ne} + ^{64}\text{Zn}$	600	$2875 \pm 130$	2873
	2000	2162	2218
	6000	$2407 \pm 200$	2133
$^{27}\text{Al} + ^{40}\text{Ca}$	1188	$2440 \pm 190$	2688
	2079	$2030 \pm 190$	2304
$^{40}\text{Ca} + ^{51}\text{V}$	1760	$2940 \pm 250$	3343
$^{40}\text{Ca} + ^{54}\text{Fe}$	1760	$3130 \pm 250$	3391
$^{40}\text{Ca} + ^{107}\text{Ag}$	1760	$4000 \pm 310$	4279
$^{40}\text{Ca} + ^{208}\text{Pb}$	1760	$5000 \pm 310$	5337
	3080	$5310 \pm 500$	5006
$^{238}\text{U} + ^{238}\text{U}$	1766	$1630 \pm 110$	2293

For a pre-equilibrium nucleus with excitation energy  $E$  and number of excitons  $n$ , the partial transition probabilities changing the exciton number by  $\Delta n$  are given by:

$$\omega_{\Delta n}(p, h, U) = \frac{2\pi}{\hbar} |M_{\Delta n}|^2 \rho_{\Delta n}(p, h, U) \quad (7)$$

here  $M_{\Delta n}$  is matrix element averaged over all possible transitions and  $\rho_{\Delta n}(p, h, E)$  is density

TABLE V: Experimental and calculated (adopted in CASCADE.04) elastic nucleus-nucleus interaction cross-sections

Nuclei	E (MeV)	$\sigma_{el}(\text{experiment})$	$\sigma_{el}(\text{calculation})$
d + $^{27}\text{Al}$	160	$594 \pm 121$	558
	650	$287 \pm 19$	354
	710	$610 \pm 120$	344
$\alpha + ^{12}\text{C}$	3480	$266 \pm 32$	245
	8400	$292 \pm 33$	291
	14400	$325 \pm 8$	302
$\alpha + ^{27}\text{Al}$	14400	$579 \pm 12$	524
$^{12}\text{C} + ^{12}\text{C}$	125	1230	1039
	150	1230	1060
	175	1230	1074
	200	1230	1077
	230	1250	1076
	290	1300	1055
	10440	$317 \pm 103$	500

of final states. The number of excitons ( $n_{eq}$ ) at the equilibrium stage is obtained by

$$\left\{ \begin{array}{l} \omega_{+2}(n_{eq}, U) = \omega_{-2}(n_{eq}, U) \\ n_{eq} = \sqrt{2gU} \end{array} \right\} \quad (8)$$

here  $g$  is the density of the single particle states which was derived with equidistant single particle levels. The level density of  $n$ -exciton state can be given as:

$$\left\{ \begin{array}{l} \rho_n(U) = \frac{g(gU)^{n-1}}{p!h!(n-1)!} \\ g \approx 0.595aA \\ a \text{ is level density parameter} \\ A \text{ is mass number} \end{array} \right\}$$

To avoid calculation of the matrix element  $|M|^2$  it was assumed in ref. [26] that transition probability  $\omega_{\Delta n=+2}(n, U)$  is the same as the probability for quasi-free scattering of a nucleon

above the Fermi level on a nucleon of the target nucleus.

$$\omega_{\Delta n}(n, U) = \frac{\langle \sigma(v_{rel}) \rangle \langle v_{rel} \rangle}{V_{int}} \quad (9)$$

here  $V_{int}$  is the interaction volume which is estimated as

$$\left\{ \begin{array}{l} V_{int} = \frac{4\pi}{3}(2r_c + \lambda) \\ v_{rel} = \sqrt{2E/m} \\ m \text{ is nucleon mass } r_c = 0.6 fm \end{array} \right\}$$

$\lambda$  is the de Broglie wave length corresponding to relative velocity  $v_{rel}$ .

$$\sigma(v_{rel}) = 0.5(\sigma_{pp}(v_{rel}) + \sigma_{pn}(v_{rel}))P\left(\frac{E_F}{E_{rel}}\right) \quad (10)$$

where factor  $P\left(\frac{E_F}{E_{rel}}\right)$  was introduced to account for Pauli principle and it is given by

$$\left\{ \begin{array}{ll} P\left(\frac{E_F}{E_{rel}}\right) = 1 - \frac{7}{5} \frac{E_F}{E_{rel}} & \text{For } \frac{E_F}{E_{rel}} \leq 0.5 \\ P\left(\frac{E_F}{E_{rel}}\right) = 1 - \frac{7}{5} \frac{E_F}{E_{rel}} + \frac{2}{5} \frac{E_F}{E_{rel}} \left(2 - \frac{E_{rel}}{E_F}\right)^{5/2} & \text{For } \frac{E_F}{E_{rel}} > 0.5 \\ E_F = 45 \text{ MeV} & \\ E_{rel} = E_P + E_N = (E_F + \frac{U}{n}) + (\frac{3}{5}E_F) & \\ E_P & \text{mean energy of projectile nucleons} \\ E_N & \text{mean energy of Target nucleons} \end{array} \right\} \quad (11)$$

The free proton-proton and proton-neutron cross-sections are estimated as given in ref [27]

$$\left\{ \begin{array}{l} \sigma_{pp}(v_{rel}) = \frac{10.63}{v_{rel}^2} - \frac{29.93}{v_{rel}} + 42.9 \text{ mb} \\ \sigma_{pn}(v_{rel}) = \frac{34.10}{v_{rel}^2} - \frac{82.20}{v_{rel}} + 82.2 \text{ mb} \end{array} \right\} \quad (12)$$

The density of final states  $\omega_{\Delta \pm 2, 0}(n, U)$  are derived by Williams [28] that was later corrected for the Pauli principle and indistinguishability of identical excitons by Ribanský, Obložinský and Bétaĕ [29] is given by

$$\left\{ \begin{array}{l} \omega_{\Delta n=-2}(n, U) = \frac{ph(n+1)(n-2)}{(gU)^2} \\ \omega_{\Delta n=0}(n, U) = \frac{(n+1)}{n} \frac{p(p-1)+4ph+n(n-1)}{gU} \\ \omega_{\Delta n=+2}(n, U) = 1 \end{array} \right\} \quad (13)$$

here the value of  $F(p, h) = (p^2 + h^2 + p - h)/4 - h/2$  is taken to 0.

The emission rate of a nucleon of the type  $i$  into the continuum is estimated according to the detailed balance principle

$$\Gamma_i(p, h, U) = \int_{V_i}^{U-B_i} \omega^i(p, h, U, E) dE \quad (14)$$

The emission probability is defined in the same manner as in the evaporation model

$$\omega(p, h, U, E) = \frac{2S_i + 1}{\pi^2 \hbar^3} \mu_i \Re(p, h) \frac{\rho(n - i, U - B_i - E)}{\rho(n, U)} \sigma_{inv} E \quad (15)$$

here  $S_i$  is spin of nucleon  $i$ ,  $\sigma_{inv}$  is the inverse cross-section from evaporation model,  $\mu_i$  is reduced mass, and  $\Re(p, h)$  takes into account the condition for the exciton to be a proton or neutron. The condensation probability for each emitting particles are obtained by fitting the theoretical pre-equilibrium spectra with the experimental data.

#### IV. EVAPORATION MODEL

The evaporation model used in CASCADE code is an extension of the Weisskopf-Ewing's model [30] by Dostrovsky et al.[31]. In order to calculate the decay width for the evaporating particles, Fermi-gas level density [32] for  $E \geq E_b$  is given by,

$$\rho(E) = \frac{c_1 \exp(2\sqrt{a(E - \delta)})}{a^{1/4}(E - \delta)^{5/4}} \quad (16)$$

and if  $E < E_b$  then constant temperature formula has been used

$$\rho(E) = c_2 \exp((E - E_0)/T) \quad (17)$$

The boundary energy  $E_b = E_0 + d$ ,  $E_0 = 2.5 + 150/A_d$  and the parameter  $1/T = \sqrt{a/E_0} - 1.5/E_0$ . The constants  $c_1, c_2$  are defined in order to have continuity of the level densities eqs 16 and 17 at boundary  $E = E_b$ . The pairing energy shift  $\delta$  is defined according to the tables given in [32, 33]. For the level density parameter we use expression [34, 35, 36] given below:

$$a(A_d, Z_d, E) = A_d(0.134 - 1.2110^{-04} A_d)(1 + \frac{S}{E}(1 - \exp(-0.061E))) \quad (18)$$

Here  $A_d$  and  $Z_d$  are the mass and charge numbers of the decayed (daughter) nucleus.  $E$  is the decaying (parent) nucleus excitation energy (MeV),  $S$  is the shell correction [32].

The evaporation probability  $P_i$  for the emission of the particle  $i$  from a parent nucleus  $j$  with total kinetic energy in the center of mass system between  $E$  and  $E + dE$  is defined (in unit of  $\hbar = c = 1$ ) by :

$$P_i = \frac{2(2S_i + 1)m_i \int_{V_i}^{U_i - B_i} \sigma_{inv} \rho_d(U_i - B_i - E) E dE}{\pi \rho_j(E)} \quad (19)$$

Here  $s_i, m_i$  and  $B_i$  are the spin, mass and binding energy of the evaporated particle. Where  $B_i = M(A_i, Z_i) + M(A_d, Z_d) - M(A_j, Z_j)$  is calculated from the mass tables given

TABLE VI:  $k$ ,  $k_\alpha$ , and  $c$  parameters adopted in CASCADE.04 from GEM [42, 43, 44]

$Z_d$	$k$	$k_\alpha$	$c$
$\leq 20$	0.51	0.81	0.0
30	0.60	0.85	-0.06
40	0.66	0.89	-0.10
$\geq 50$	0.68	0.93	-0.10

in [37, 38] and we use Cameron's mass formula [39] where such values are not available in tables [38],  $U$  is the excitation energy of the decaying (parent) nucleus. The cross-section of inverse reaction or cross-section for particle evaporation is given as:

$$\sigma_{inv} = \pi R^2 \alpha \left(1 + \frac{\beta}{E}\right) \quad (20)$$

Here the constants  $\beta$  and  $\alpha$  are calculated by fitting the expression to the theoretical calculation done by Shapiro [40] and, Blatt and Weisskopf [41] in order to take the effect of overlapping wave function. These constants given in [42, 43, 44] are listed below in VI. The above formula (eq. 20) can be written for neutron as:

$$\sigma_{inv} = \pi R_b^2 c_n \left(1 + \frac{b}{E}\right) \quad (21)$$

and for charged particles as:

$$\sigma_{inv} = \pi R_b^2 c_i \left(1 - \frac{V_i}{E}\right) \quad (22)$$

The nuclear distance ( $R_g$ ) is given by;  $R_g = 1.5A_d^{1/3}$  for neutron and proton and,  $1.5(A_d^{1/3} + A_j^{1/3})$  for d, t,  $^3\text{He}$ , and  $\alpha$ . Coulomb barrier is given as:

$$V_i = \frac{1.44K_i Z_i (Z - Z_i)}{R_0 A^{1/3} + r} \quad (23)$$

Here  $R_0 = 1.7$  and  $r = 0$  for neutron and proton, and  $r = 1.2$  for d, t,  $^3\text{He}$ , and  $\alpha$ . For all light ejectiles up to ( $A_j \leq 4$ ), parameters determined by S. Furihata realized in code GEM are  $c_n = 0.76 + c_a A_d^{-1/3}$ ,  $b = (b_a A_d^{2/3} - 0.050)/(0.76 + c_a A_d^{-1/3})$  (and  $b = 0$  for  $A_d \geq 192$ ), where  $c_a = 1.93$  and  $b_a = 1.66$ ,  $c_p = 1 + c$ ,  $c_d = 1 + c/2$ ,  $c_t = 1 + c/3$ ,  $c^3\text{He} = c_\alpha = 0$ ,  $k_p = k$ ,  $k_d = k + 0.06$ ,  $k_t = k + 0.12$ ,  $k^3\text{He} = k_\alpha - 0.06$ , where  $c$ ,  $k$ , and  $k_\alpha$  are listed in table VI for a set of  $Z_d$ .  $c$ ,  $k$ , and  $k_\alpha$  are obtained by linear interpolation between the  $Z_d$  values listed in table VI.

In the precursor of the CASCADE.04 code, we have included ejectiles up to  $^4\text{He}$  at the evaporation stage but in CASCADE.04 66 ejectiles, not only in their ground state but also

TABLE VII: The particles considered to be emitted at evaporation stage

$Z_i$							
0	n						
1	p	d	t				
2	$^3\text{He}$	$^4\text{He}$	$^6\text{He}$	$^8\text{He}$			
3	$^6\text{Li}$	$^7\text{Li}$	$^8\text{Li}$	$^9\text{Li}$			
4	$^7\text{Be}$	$^9\text{Be}$	$^{10}\text{Be}$	$^{11}\text{Be}$	$^{12}\text{Be}$		
5	$^8\text{B}$	$^{10}\text{B}$	$^{11}\text{B}$	$^{12}\text{B}$	$^{13}\text{B}$		
6	$^{10}\text{C}$	$^{11}\text{C}$	$^{12}\text{C}$	$^{13}\text{C}$	$^{14}\text{C}$	$^{15}\text{C}$	$^{16}\text{C}$
7	$^{12}\text{N}$	$^{13}\text{N}$	$^{14}\text{C}$	$^{15}\text{N}$	$^{16}\text{N}$	$^{17}\text{N}$	
8	$^{14}\text{O}$	$^{15}\text{O}$	$^{16}\text{O}$	$^{17}\text{O}$	$^{18}\text{O}$	$^{19}\text{O}$	$^{20}\text{O}$
9	$^{17}\text{F}$	$^{18}\text{F}$	$^{19}\text{F}$	$^{20}\text{F}$	$^{21}\text{F}$		
10	$^{18}\text{Ne}$	$^{19}\text{Ne}$	$^{20}\text{Ne}$	$^{21}\text{Ne}$	$^{22}\text{Ne}$	$^{23}\text{Ne}$	$^{24}\text{Ne}$
11	$^{21}\text{Na}$	$^{22}\text{Na}$	$^{23}\text{Na}$	$^{24}\text{Na}$	$^{25}\text{Na}$		
12	$^{22}\text{Mg}$	$^{23}\text{Mg}$	$^{24}\text{Mg}$	$^{25}\text{Mg}$	$^{26}\text{Mg}$	$^{27}\text{Mg}$	$^{28}\text{Mg}$

in excited state, as it was suggested by [45] are included. This consideration enhances the yield of heavy particles evaporation. The 66 ejectiles taken into consideration at evaporation stage are selected to satisfy the following criteria: (1) isotopes with  $Z_i = 12$ ; (2) naturally existing isotopes or isotopes near the stability line; (3) isotopes with half-lives longer than 1 ms. All the 66 ejectiles considered are given in table VII.

For fragments heavier than  $^4\text{He}$ , the following parameters are used;  $c_i=k_i=1$ ,  $R_g=R_0(A_i)+R_0(A_d)+2.85$  [fm],  $R=R_0(A_i)+R_0(A_d)+3.75$  [fm], where  $R_0(A)=1.12A^{1/3}-0.86A^{-1/3}$ . An excited state of a fragment particle is included in calculations if its half lifetime satisfies the following condition:

$$\frac{T_{1/2}}{\ln 2} = \frac{\hbar}{\Gamma_i^*} \quad (24)$$

Where  $\Gamma_i^*$  is the decay width of the excited particle (at resonance).  $\Gamma_i^*$  is calculated in the same manner as for a ground-state particle emission. The Q-value for the excited particle emission is given as  $B^* = B_{ground} + E_i^*$ , where  $E_i^*$  is the energy of excited state. The mass of the excited state is taken same as of ground state because of negligible difference in their masses. The spin of the excited state  $S_i^*$  is used in the calculation of  $\Gamma_i$ , instead of the

spin of the ground state  $S_i$  as the spin differ significantly from the ground state. Instead of treating an excited state as an independent particle, we simply enhances the decay width  $\Gamma_i^*$  (as in GEM) of the ground state particle emission as follows:

$$\Gamma_i = \Gamma_i^0 + \sum_n \Gamma_i^n \quad (25)$$

Here  $\Gamma_i^0$  is the decay width of the ground state particle emission, and  $\Gamma_i^n$  is that of the n-th excited state of i-th particle emission which satisfies the condition as in eq.25.

In the present version of the evaporation model realized in CASCADE.04 code we have three options, 1) ejectiles up to  $^4\text{He}$  with the new constants for Coulomb energy and inverse cross-section as realized in GEM which are slightly different from the Dostrovsky's constants, 2) all ejectiles given in Table VII in their ground state and, 3) all ejectiles in their excited state.

The third option is only important to calculate the cross-section for heavy ejectiles or for some particular problems but it affects the spallation and fission yield cross-section for preactinide elements negligibly and it affects slightly to the spallation cross-section for the actinides. Thus in the most cases, one may restrict oneself up to six particles: n, p, d, t,  $^3\text{He}$ ,  $^4\text{He}$ . Consideration of such heavy ejectiles demands a large CPU time because one must take into account an emission of fragments in various excitation (resonance) states. As we mentioned above the problem of swelling from the production of oxygen, helium and other gases, one can use our program for such investigation and for another problem one may avoid it to save the time of simulation.

The total kinetic energy distribution of the excited particles is calculated in the same manner as of the ground state particle. The data for the excited state are extracted from the Evaluated Nuclear Structure Data File (ENSDF) database maintained by the National Nuclear Data Center at Brookhaven National Laboratory.

As level density parameter is energy dependent the probability of evaporation and fission are calculated now exactly - by means of numerical integration instead of customary use of some approximate expressions. Sampling of the energy of a particle emitted by residual nucleus has been done taking into account eqs. 16 and 17.

## V. FISSION MODEL

The probability of fission  $P_f$  in competition to evaporation is calculated as given below (in unit of  $h = c = 1$ ):

$$P_f = \frac{\int_0^{U-B_f} \rho(U - B_f - \delta - E) dE}{\rho_j(E)} \quad (26)$$

Calculations have shown that agreement with experiment is better if in case of the fission the level density parameter  $a_f$  is higher than at that at evaporation  $a_n$ .

$$a_f = a_n \left\{ \begin{array}{ll} 1.041 + 0.00915X^2 - 0.0005977X^3 & \text{For } Z < 78 \\ 1.0196 + 0.00896X^2 - 0.000585X^3 & \text{For } 78 < Z < 85 \\ 0.9445 + 0.0083X^2 - 0.000542X^3 & \text{For } Z > 85 \end{array} \right\} \quad (27)$$

here  $X=Z^2/2-30.893$ . This empirical approach good fitted to make better agreement of mass-distribution produced in fission with experimental data.

We have taken the fission barrier  $B_f$  calculated according to the formulation [46] which is in better agreement with the experimentally measured fission barriers within  $\pm 0.5\text{MeV}$ . The Thomas-Fermi fission barrier formulation is given below:

$$\left\{ \begin{array}{ll} B_f(N, Z) = S(N, Z)F(X) & [\text{MeV}] \\ S(N, Z) = A^{2/3}(1 - kI^2) \\ k = 1.9 + \frac{Z-80}{75} \\ I = \frac{(N-Z)}{A} \\ X = \frac{Z^2}{A(1-kI^2)} \\ F(X) = 0.0001999749(X_0 - X)^3 & \text{For } X_1 \leq X \leq X_0 \\ F(X) = 0.595553 - 0.124136(X - X_1) & \text{For } 30 \leq X \leq X_1 \\ \text{here } X_0 = 48.5428 & \text{and } X_1 = 34.15 \end{array} \right\} \quad (28)$$

here  $S$  is approximately proportional to surface energy and  $k$  is surface symmetry coefficient and is given by a function of  $Z$ , the fissility  $X$  is taken as the ratio of the nominal coulomb and surface energies of a sphere.

The CASCADE uses the statistical model of fission [47] which defines the probability of a possible mode of fission by density of quantum states of total excitation energy  $E$ . The density of quantum states of fission fragments  $A_1$  with excitation energy  $E_1$  and  $A_2$  with excitation energy  $E_2$  is calculated as the product of their level densities. Level densities of

these fission fragments are given as:

$$\left\{ \begin{array}{l} \Omega(E_1) = c_1 \exp(2\sqrt{a_1 E_1}) \\ \Omega(E_2) = c_2 \exp(2\sqrt{a_2 E_2}) \end{array} \right\} \quad (29)$$

The fission theory given by Fong takes into account the complete equilibrium condition at scission, as given below:

$$E_1 : E_2 = a_1 T^2 : a_2 T^2 = a_1 : a_2 \quad (30)$$

According to the Fong's theory, the masses of the fission fragments are decided at the scission point. At scission point when two fragments are in contact they have equal temperature as shown in 29. By eqs. 29 and 30 we can write the total density of states as given below

$$\Omega(E) = c_1 c_2 \int_0^E \exp(2\sqrt{(a_1 + a_2)(E_1 + E_2)}) \quad (31)$$

here  $E=E_1+E_2$ . The excitation energy of the fissioning nuclei is calculated by  $E = M^*(A, Z) - M(A_1, Z_1) - M(A_2, Z_2) - \text{coulomb energy} - \text{deformation energy}$ . Deformation energy is given as:

$$D(i) = (0.4E_S - 0.2E_C)\alpha_{2i}^2 + (0.7144E_S - 0.204E_C)\alpha_{3i}^2 \quad (32)$$

Here  $E_S = 20.76A_i^{2/3}$  is the surface energy,  $E_C = 0.7354Z^2/A_i^{1/3}$  is the coulomb potential,  $\alpha_{2i}$  and  $\alpha_{3i}$  are the deformation parameters calculated by liquid drop model with the condition of minimum potential energy (the most probable fission mode). Coulomb energy of the deformed nucleus is calculated as:

$$\left\{ \begin{array}{l} V_C = \frac{1.44Z_1Z_2}{R_{12}} \quad [\text{MeV}] \\ R_{12} = R_0(1 + \alpha_{2i}(1 - \frac{3}{5}X_i) + \alpha_{3i}(1 - \frac{3}{7}X_i^2)) \\ X_i = \frac{R_0(i)}{\sum_i R_0(i)(1 + \alpha_{2i} + \alpha_{3i} - \frac{9}{35}\alpha_{2i}\alpha_{3i})} \\ R_0(i) = R_0A_i^{1/3} \quad \text{and } R_0 = 1.3 \end{array} \right\} \quad (33)$$

The non zero value helps us to increase the width of the fission fragment mass yield distribution slightly 5

The available excitation energy for the possible splinters is calculated with  $E = \Delta M - D(1) - D(2) - V_C$  here  $D(i)$  ( $i=1,2$ ) are the splinters deformation energies,  $V_C$  is the Coulomb interaction energy of splinters given above and  $\Delta M$  is the difference of the fissioning nucleus and splinters masses. The equation 31 was applied to calculate the mass, charge, kinetic energy and the other fission splinters parameters. The agreement of the model depends on the input data (nuclear masses, level densities) and initial parameters to calculate the deformation and coulomb energies.

The yield of the symmetric fission products increases with increasing energy but the most probable mode of fission remains the most probable. The mode of fission depends on the density of quantum states of a nuclear system which depend on the excitation energy (masses, coulomb energy and deformation energy). Strong evidence has been found for different thresholds of the symmetric and asymmetric fission components [48, 49] which demonstrate the influence of the saddle-point configuration on the fission-fragment distribution. The competition of different fission components as a function of the excitation energy has been explained by the temperature dependence of shell effects [50, 51]. This seems that the population of the fission valleys is determined earlier than reaching the scission configuration or that the complete equilibrium does not reach while deciding the fission fragments. Thus we excluded the complete equilibrium condition used in Fong's theory [47]. To do this, integration has been taken for all partial level densities as given below:

$$\Omega(E) = c_1 c_2 \int_0^E \exp(2\sqrt{a_1(E_1 - \delta)}) \exp(2\sqrt{a_2(E - E_1 - \delta)}) \quad (34)$$

$$\left\{ \begin{array}{ll} \delta = \chi \cdot \frac{14}{\sqrt{A}} \\ \chi = 2 & \text{For even-even} \\ \chi = 1 & \text{For odd-even or even-odd} \\ \chi = 0 & \text{For odd-odd} \end{array} \right\} \quad (35)$$

$\delta$  is pairing energy correction. The constant outside the integration in eq.34 can be calculated with the momentum conservation although the magnitude of the constant outside the integration is much smaller than the exponential factor. The Total density of states of nuclei A into masses  $(A_1, E_1)$ ,  $(A_2, E_2)$  with total excitation energy E, considering angular momentum conservation and momentum states of the two nuclei can be given as:

$$\left\{ \begin{array}{l} \Omega(A_1, A_2) X_1 X_2 \int_0^E \exp(2\sqrt{a_1(E_1 - \delta)}) \exp(2\sqrt{a_2(E - E_1 - \delta)}) \\ X_1 = \left\{ \frac{A_1^{5/3} A_2^{5/3}}{A_1^{5/3} + A_2^{5/3}} \right\}^{3/2} \left\{ \frac{(E_1 + E_2)}{(a_1 + a_2)} \right\}^{3/4} \\ X_2 = \left\{ \frac{A_1 A_2}{A_1 + A_2} \right\}^{3/2} \left\{ \frac{(E_1 + E_2)}{(a_1 + a_2)} \right\}^{3/4} \end{array} \right\} \quad (36)$$

Here  $X_1$  represents the angular momentum conservation,  $X_2$  momentum states and, integration has been taken for all partial level densities.  $a_1$  and  $a_2$  are the level density parameters as given in eq.18. Evaporation from fission fragments is also considered in usual manner if enough excitation energy is available for evaporation.

Charge distribution: One can consider the charge distribution in a very simple manner as given in [5]. We have also considered that the charge can be calculated having the same neutron to proton ratio for the fragments as it was for the fissioning nucleus.

Kinetic energy distribution: Kinetic energy of the fragments is calculated from the available excitation energy in their mass ratio.

## VI. BENCHMARK OF THE CODE FOR ISOTOPE PRODUCTION CROSS-SECTIONS

The CASCADE code has been designed to simulate for thin as well as thick targets. In case of thin target, the code simulates collision only for single nucleus. A list of all the isotopes, integrated charge, and mass number distributions are generated in the output file. The isotope distributions are compared for the  $p(0.3\text{GeV and }1.0\text{GeV})+^{56}\text{Fe}$ ,  $p(0.5\text{ and }1.0\text{GeV})+^{208}\text{Pb}$ , and  $p(1.0\text{GeV})+^{238}\text{U}$  reaction for that a full list of the data are available from the method of inverse kinematics (magnetic spectroscopy).

The ratio of the calculated and Experimental yield data are plotted for each isotopic distribution. A general observation, as seen from the Figures (7,8,9, and 10) is that the theoretical values are in good agreement with the experimental data close to the target mass number as well as at the peak of the isotopic distribution but the disagreement increases at the tail of the distribution. The width of the calculated distributions are less compared to the experimental data almost in all cases. It is to be noticed that even-odd effect is still seen in the code calculations which are absent in the experimental data. The pairing correction is included in the calculation which reduces the effect but does not vanish completely. The deep spallation region that comes after a long chain of the multi-step direct and evaporation mechanism, is underestimated by the present version of the code. It is to be noted that these calculation are shown for the case where particle emission up to alpha are considered. The ratio of the calculated and Experimental yield data are plotted for each isotopic distribution. A general observation, as seen from the Figures (7,8,9, and 10) is that the theoretical values are in good agreement with the experimental data close to the target mass number as well as at the peak of the isotopic distribution but the disagreement increases at the tail of the distribution. The width of the calculated distributions are less compared to the experimental data almost in all cases. It is to be noticed that even-odd effect is still seen in the code calculations which are absent in the experimental data. The pairing correction is included in the calculation which reduces the effect but does not vanish completely. The deep spallation region that comes after a long chain of the multi-step direct and evaporation mechanism, is underestimated by the present version of the code. It is to be noted that these calculation are shown for the case where particle emission up to alpha are considered.

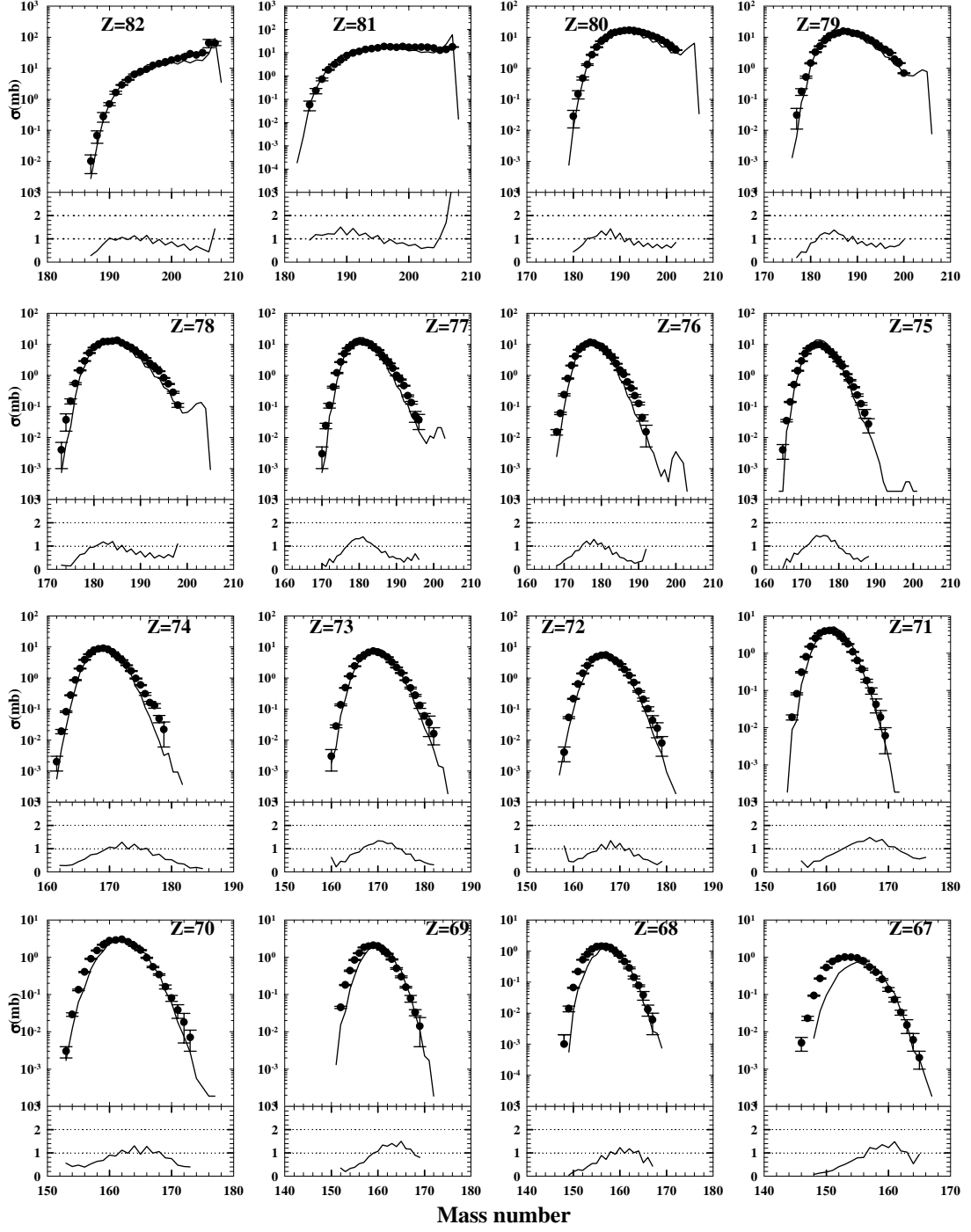


FIG. 7: Comparison of calculated isotope production cross-sections for  $p(1\text{GeV})+^{208}\text{Pb}$  reaction with experimental data [52].

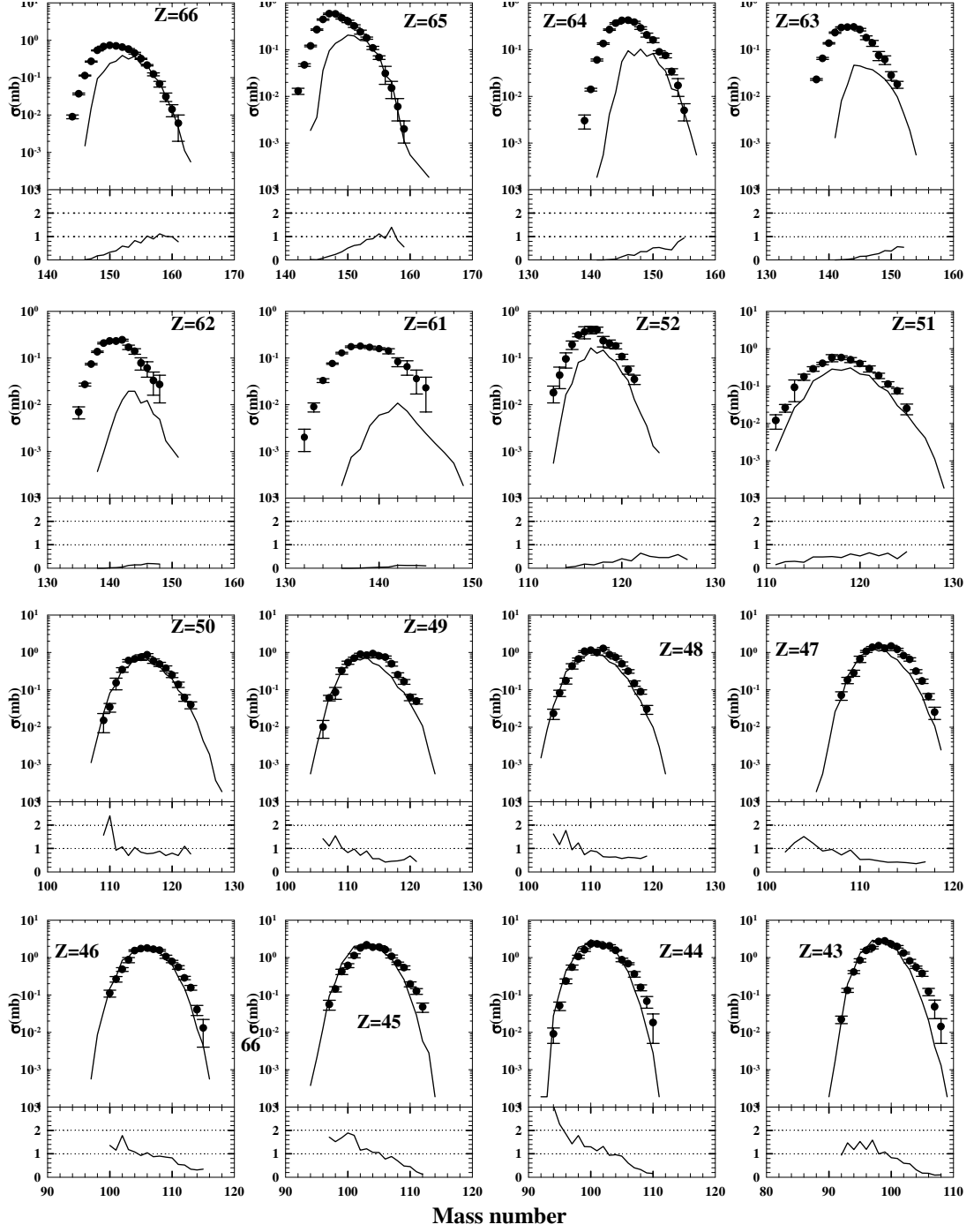


FIG. 8: Same as Figure 7.

The ratio of the calculated and Experimental yield data are plotted for each isotopic distribution. A general observation, as seen from the Figures (7,8,9, and 10) is that the theoretical values are in good agreement with the experimental data close to the target mass number as well as at the peak of the isotopic distribution but the disagreement increases at

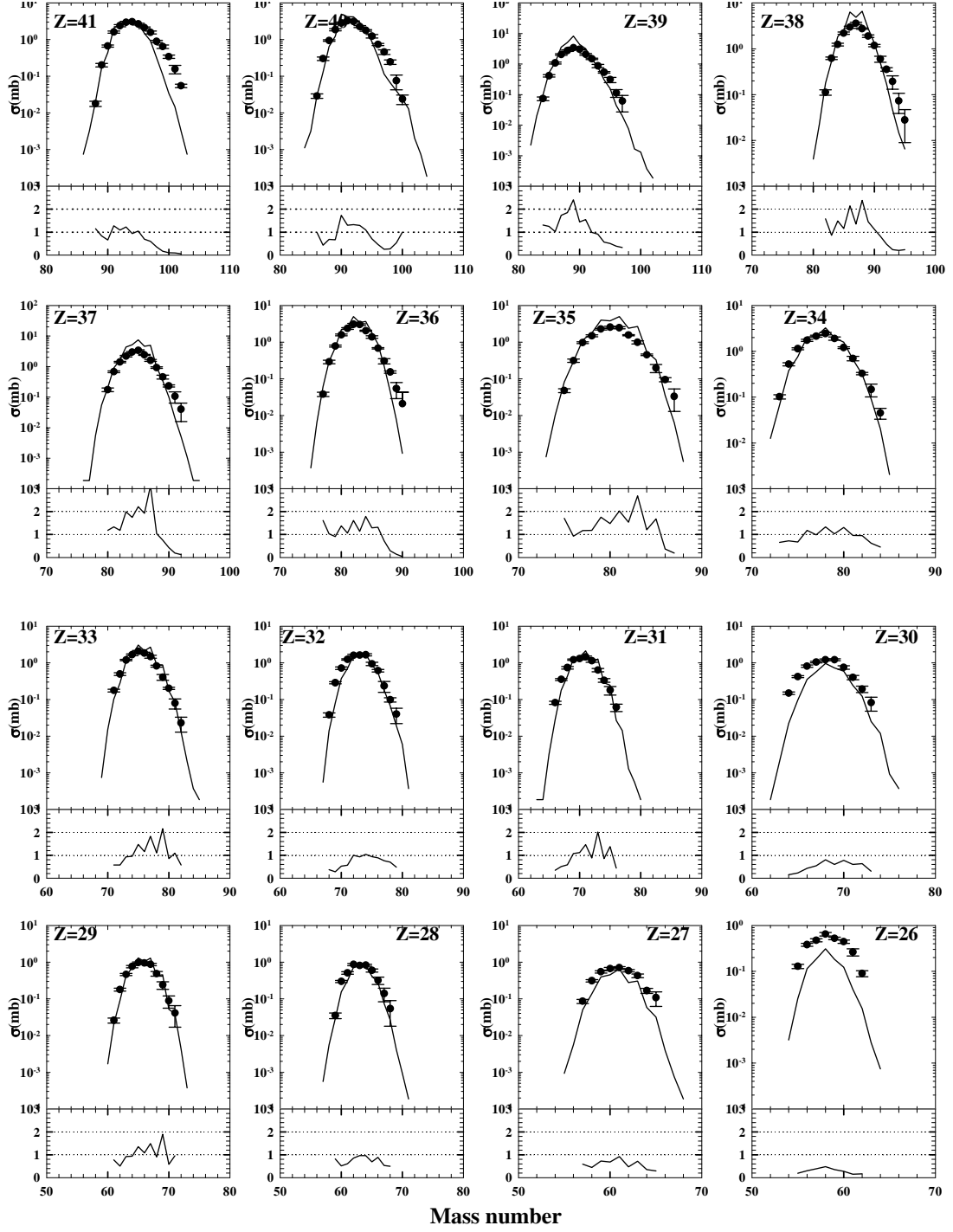


FIG. 9: Same as Figure 7.

the tail of the distribution. The width of the calculated distributions are less compared to the experimental data almost in all cases. It is to be noticed that even-odd effect is still seen in the code calculations which are absent in the experimental data. The pairing correction is included in the calculation which reduces the effect but does not vanish completely. The

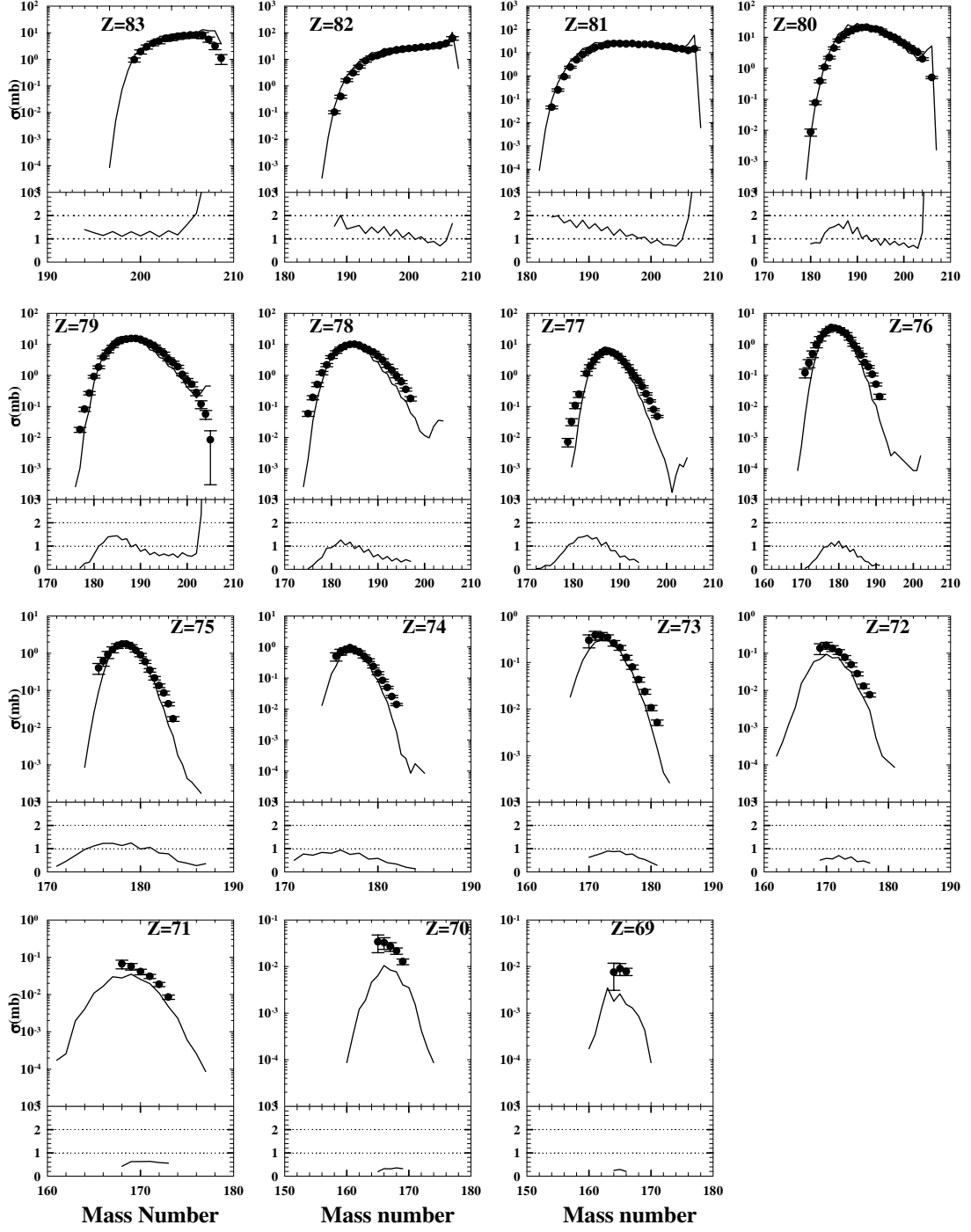


FIG. 10: Comparison of calculated isotope production cross-sections for  $p(500\text{MeV}) + {}^{208}\text{Pb}$  reaction with experimental data [53]

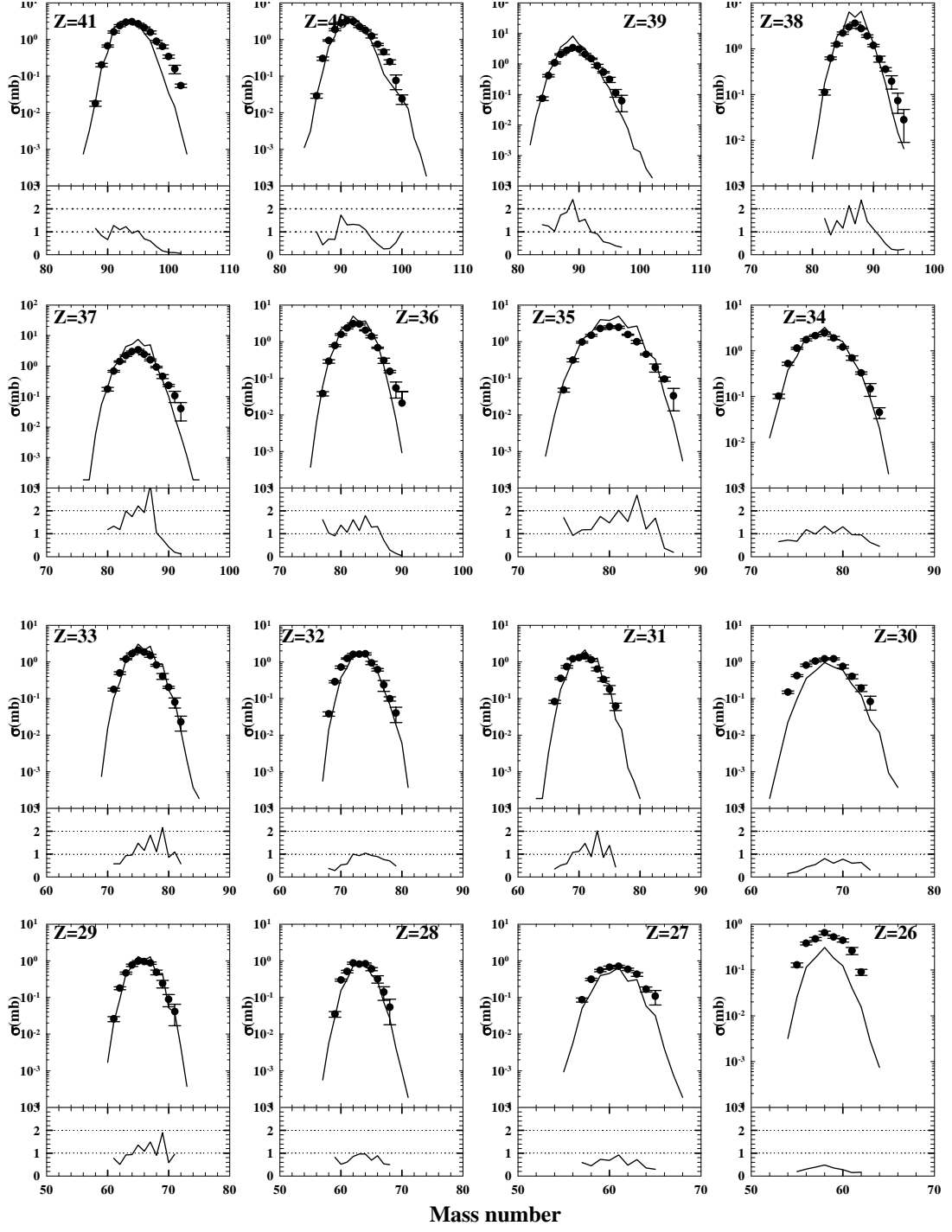


FIG. 11: Comparison of calculated isotope production cross-sections for  $p(1\text{GeV})+^{238}\text{U}$  reaction with experimental data [54, 55, 56, 57]

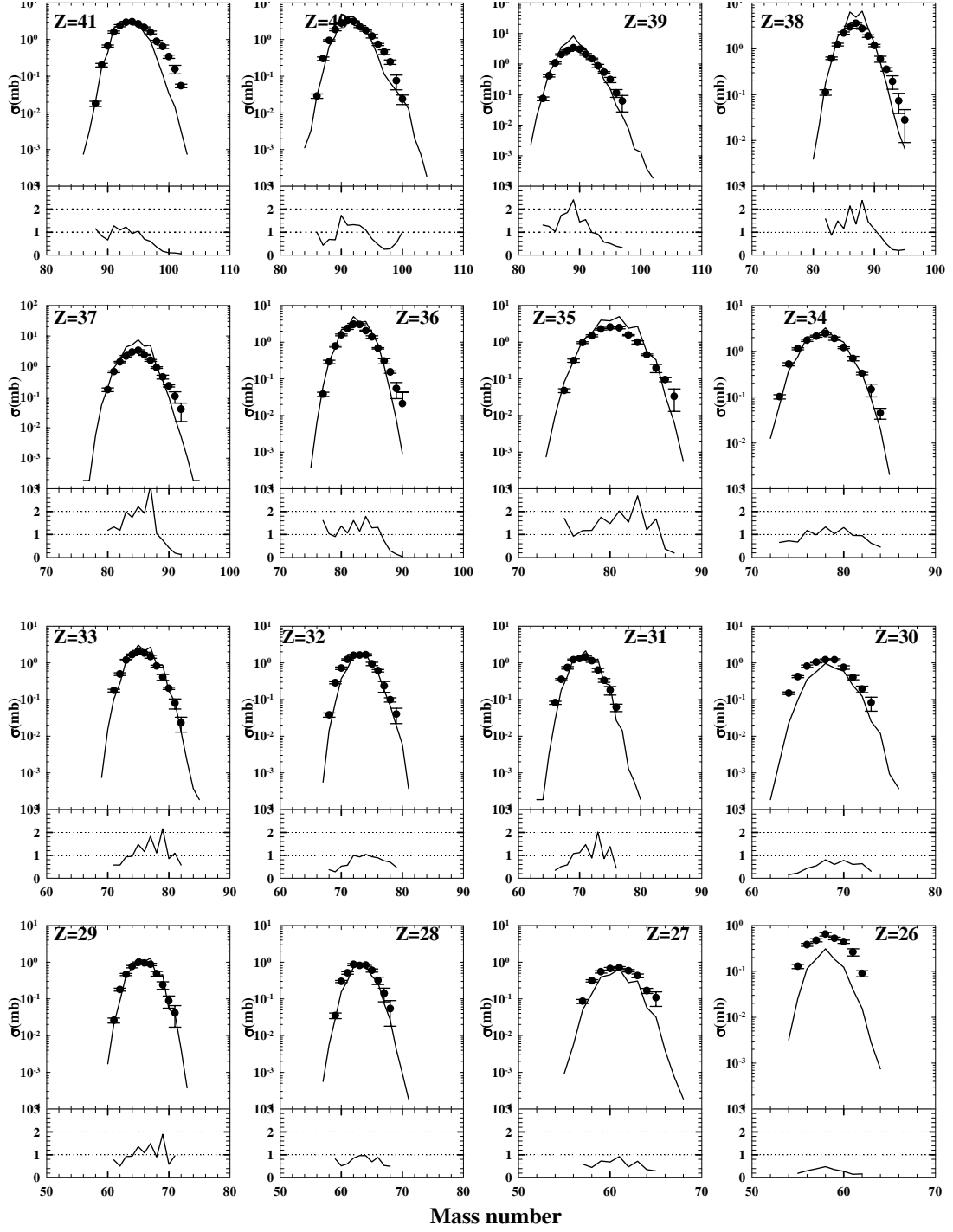


FIG. 12: Same as Figure 11.

deep spallation region that comes after a long chain of the multi-step direct and evaporation mechanism, is underestimated by the present version of the code. It is to be noted that these calculation are shown for the case where particle emission up to alpha are considered.

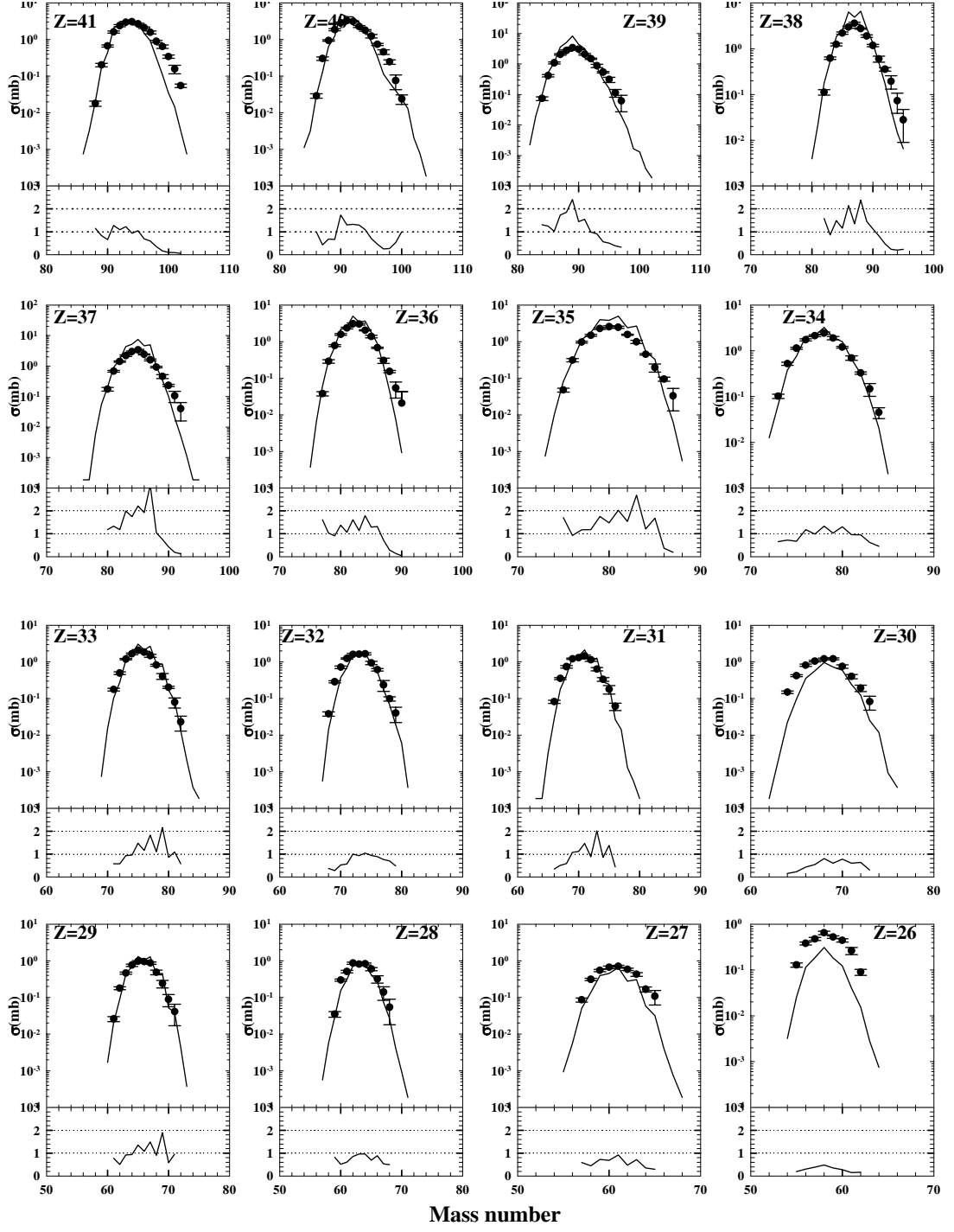


FIG. 13: Same as Figure 11.

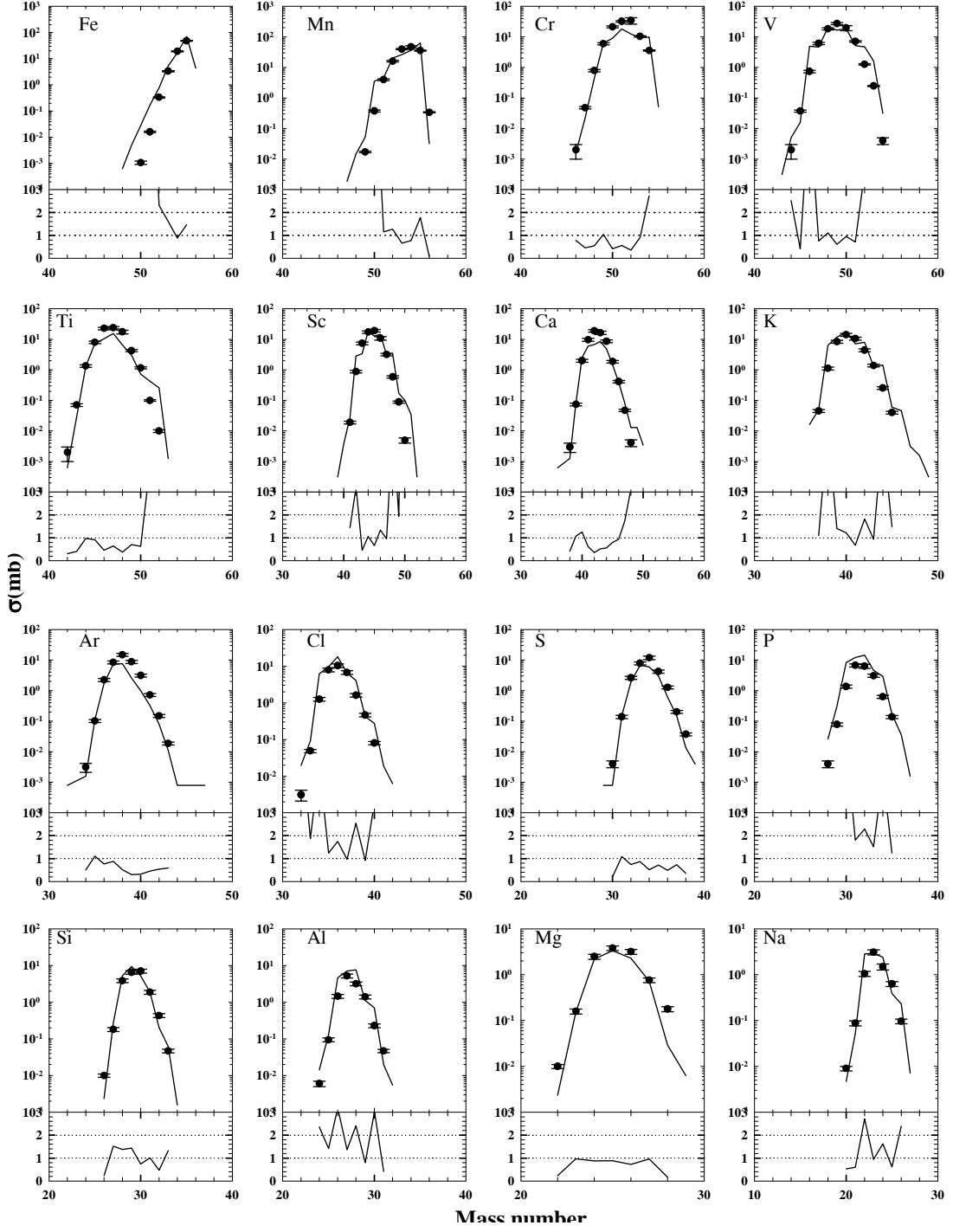


FIG. 14: Comparison of calculated isotope production cross-sections for  $p(1\text{GeV})+^{56}\text{Fe}$  reaction with experimental data [58]

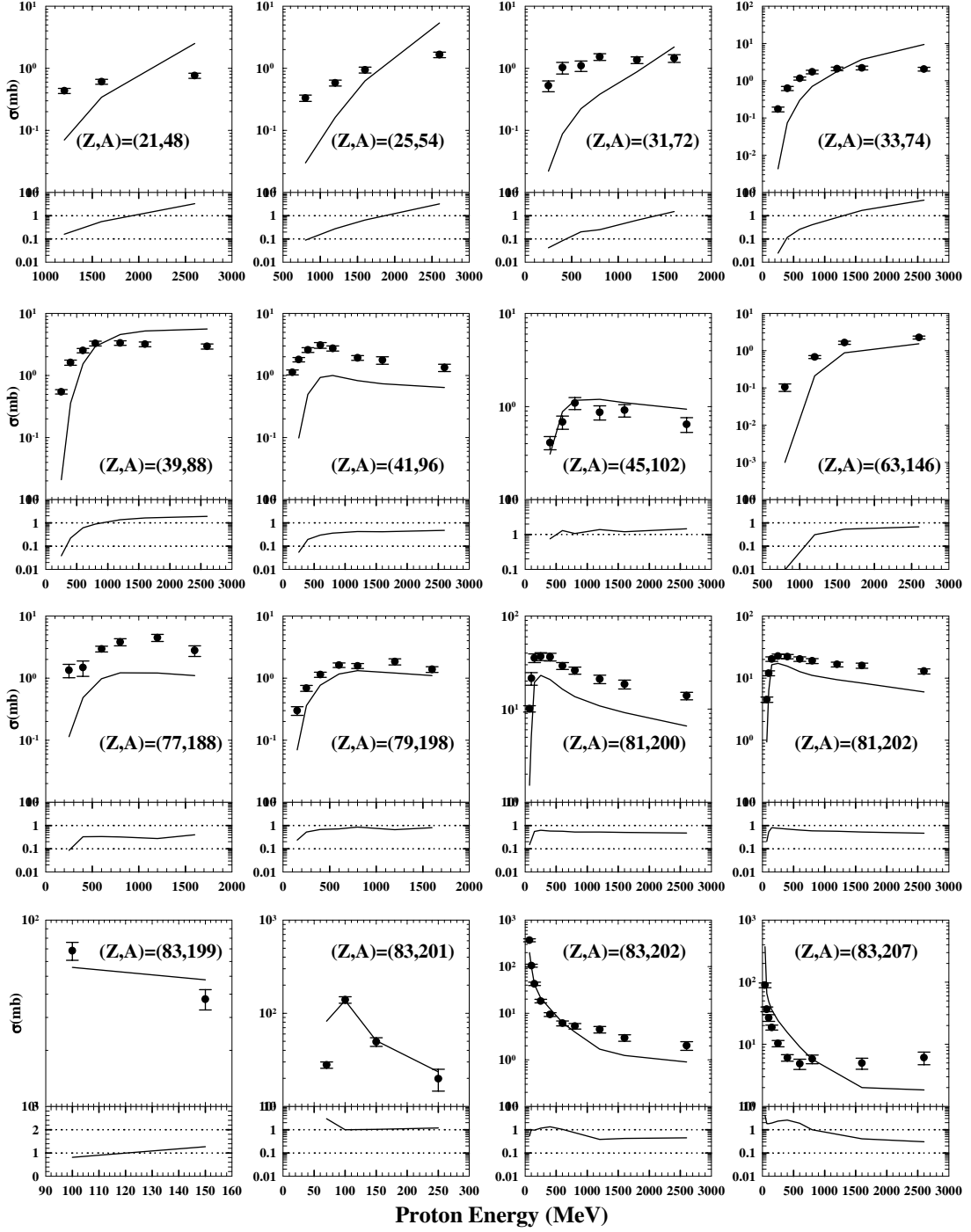


FIG. 15: Comparison of calculated excitation functions of independent yield for  $p+^{208}\text{Pb}$  reaction with experimental data [59]

## VII. BENCHMARK OF THE CODE FOR EXCITATION FUNCTIONS

## VIII. BENCHMARK OF THE CODE FOR NEUTRON DOUBLE DIFFERENTIAL CROSS-SECTIONS

## IX. BENCHMARK OF THE CODE FOR CHARGE PARTICLES DOUBLE DIFFERENTIAL CROSS-SECTIONS

## X. BENCHMARK OF THE CODE FOR PIONS PARTICLES DOUBLE DIFFERENTIAL CROSS-SECTIONS

## XI. THICK TARGET CALCULATIONS

## XII. CONCLUSIONS

### Acknowledgments

- 
- [1] R. Sternheimer, Phys. Rev. **145**, 247 (1966).
  - [2] R. Sternheimer, Phys. Rev. **B 3**, 3681 (1971).
  - [3] L. Lindhard *et al.*, Kon. Dan. Vidensk. Selsk. Nat.-Fys. Medd. **33**, 14 (1963).
  - [4] V. Barashenkov *et al.*, Phys. Part. Nucl. **24**, 107 (1993).
  - [5] V. Barashenkov and V. Toneev, Atomizdat, Moscow, 1972.
  - [6] V. Barashenkov, Comp. Phys. Commun. **126**, 38 (2000).
  - [7] V. Barashenkov, JINR P2-81-364, Dubna, 1981.
  - [8] V. Barashenkov, JINR, Dubna, 1993.
  - [9] V. Barashenkov and A. Polanski, JINR E2-94-417, Dubna, 1994.
  - [10] V. Barashenkov and H. Kumawat, Kerntechnik **68**, 259 (2003).
  - [11] S. Mashnik and V. Toneev, JINR p4-9417, Dubna, 1974.
  - [12] A. M. M. Blann and W. Scobel, Nucleonika **21**, 335 (1976).
  - [13] L. Abagian *et al.*, Energoatomizdat, Moscow, 1981.
  - [14] H. Kumawat and V. Barashenkov, Euro. Phys. J **A 26**, 61 (2005).
  - [15] V. Toneev and K. Gudima, Nucl. Phys. **A400**, 173c (1983).
  - [16] R. Serber, Phys. Rev. **72**, 1114 (1947).

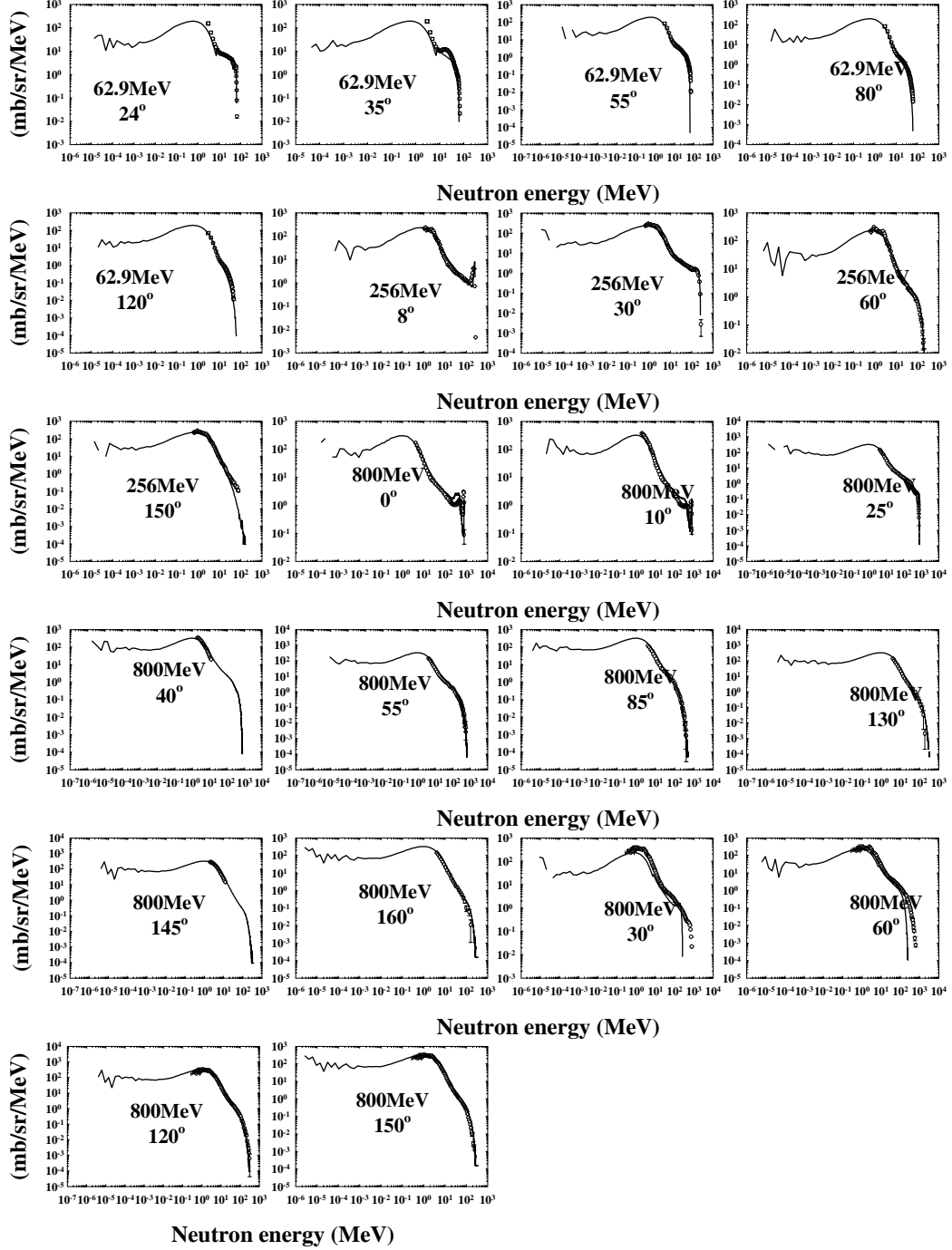


FIG. 16: Comparison of calculated neutron production cross-sections for  $p(62.9\text{MeV}, 256\text{MeV}, \text{ and } 800\text{MeV}) + {}^{208}\text{Pb}$  reaction with experimental data [60, 61]

[17] S. Gupta and S. Kailas, Z. Phys. **317**, 75 (1984).

[18] R. Glauber, Lectures in Theoretical Physics. Vol. 1, ed. Brittin (Inter-science, New York, 1959) p. 315.

[19] R. Bass, Nuclear Reactions with Heavy Ions (Springer, Berlin, 1980).

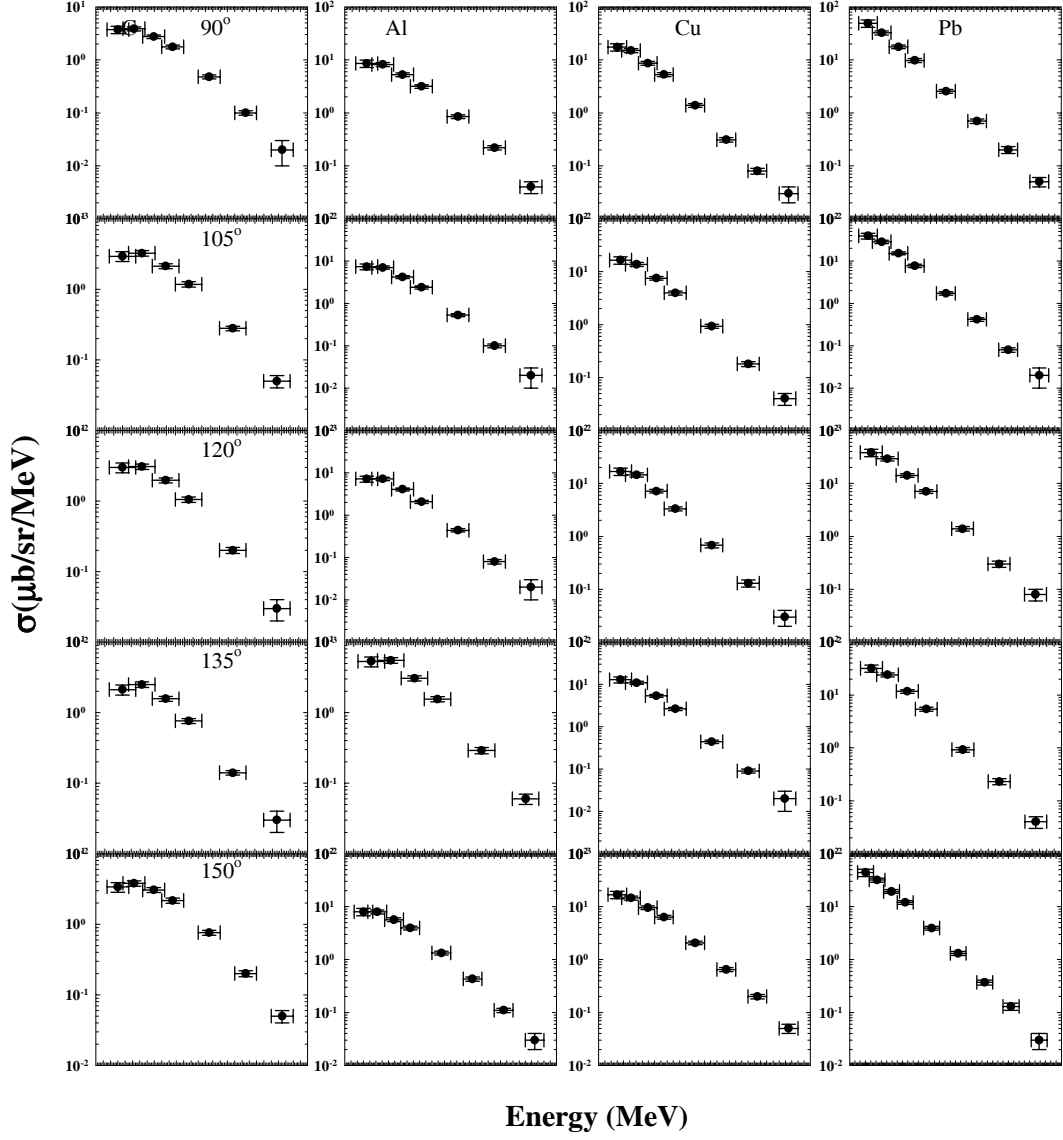


FIG. 17: Comparison of calculated isotope production cross-sections for  $p(1\text{GeV})+^{238}\text{U}$  reaction with experimental data [54, 55, 56, 57]

- [20] J. Wilson *et al.*, NASA RP-1257, December 1991.
- [21] L. Townsend and J. Wilson, *Rad. Res.* **106**, 283 (1986).
- [22] L. Sihver *et al.*, *Phys. Rev. C* **47**, 1225 (1993).
- [23] S. Kox *et al.*, *Phys. Rev. C* **35**, 1678 (1987).
- [24] C. Wong *et al.*, *Phys. Rev. Lett.* **31**, 766 (1973).
- [25] u.D. Kibkalo, *Ukr. Phys. J.* **25**, 1565 (1980).
- [26] S. M. K.K. Gudima and V. Toneev, *Nucl. Phys. A* **401**, 329 (1983).
- [27] N. Metropolis *et al.*, *Phys. Rev.* **100**, 185 (1958).

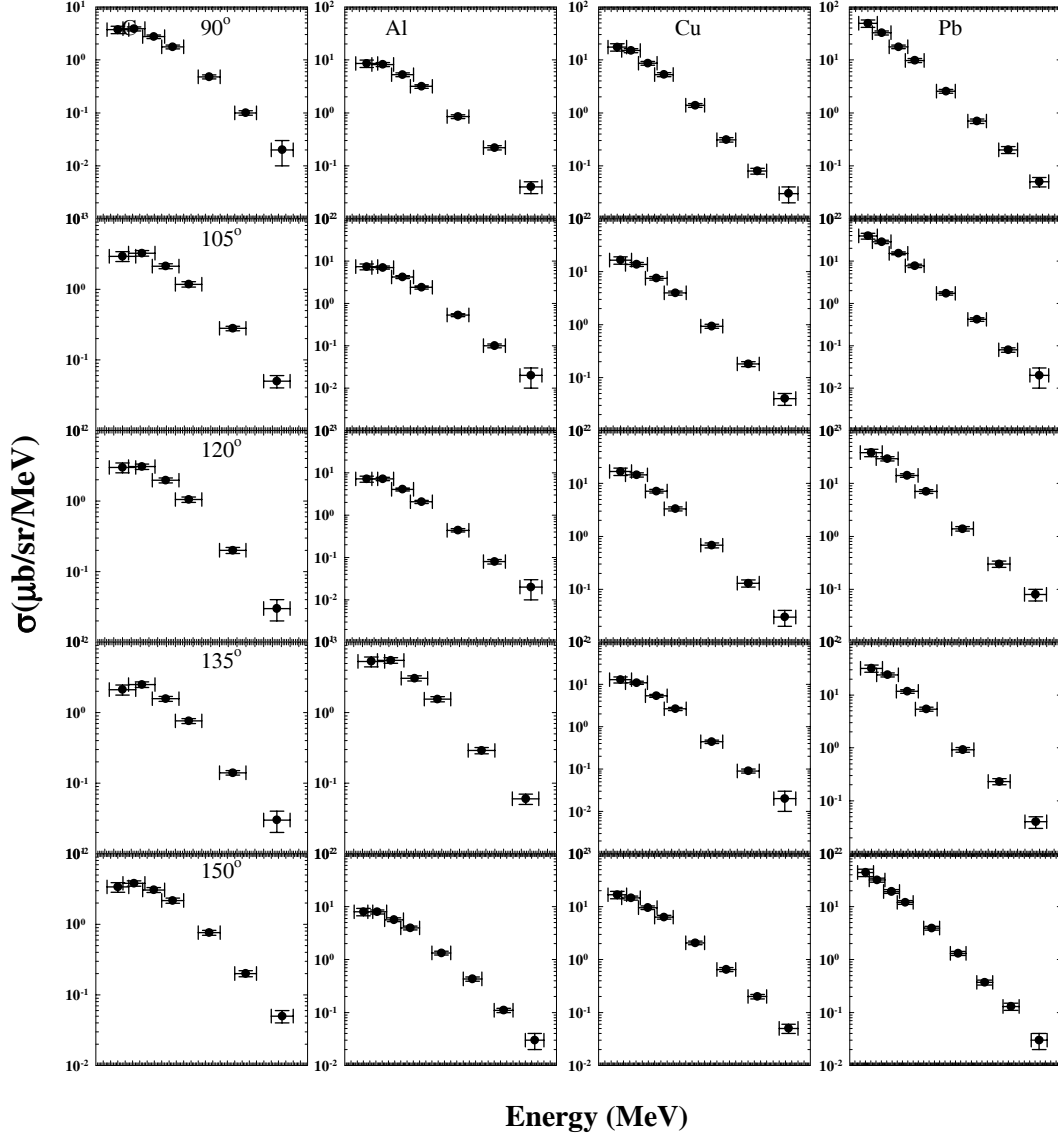


FIG. 18: Comparison of calculated isotope production cross-sections for  $p(1\text{GeV})+^{238}\text{U}$  reaction with experimental data [54, 55, 56, 57]

- [28] F. C. Williams, Nucl. Phys. **A205**, 545 (1973).
- [29] P. I. Ribanský and E. Bétaĕ, Phys. Lett. **B31**, 180 (1970).
- [30] V. Weisskopf and P. Ewing, Phys. Rev. **57**, 472 (1940).
- [31] Z. F. I. Dostrovsky and G. Friedlander, Phys. Rev. **116**, 683 (1959).
- [32] A. Gilbert and A. Cameron, Can. J. Phys. **43**, 1446 (1965).
- [33] H. F. J. L. Cook and A. Musgrove, Aust. J. Phys. **20**, 477 (1967).
- [34] E. Cherepanov and A. Ilinov, Nucleonika **25**, 611 (1980).
- [35] G. S. A. V. Ignatyuk and A. Tishin, Yad. Fiz. **21**, 485 (1975).

- [36] S. Mashnik, Acta Phys. Slov. **43**, 96 (1993).
- [37] G. Audi and A. Wapstra, Nucl. Phys. **A565**, 1 (1993).
- [38] <http://ie.lbl.gov/mass/2003AWMass-3.pdf>.
- [39] A. Cameron, Can. J. Phys. **35**, 1021 (1957).
- [40] M. Shapiro, Phys. Rev. **90**, 171 (1953).
- [41] J. Blatt and V. Weisskopf, Theoretical Nuclear Physics, Jonh Wiley Sons Inc., New York 1952.
- [42] S. Furihata, Nucl. Instr. Meth. Phys. Res. **B 171**, 251 (2000).
- [43] S. Furihata, Proc. Monte Carlo 2000 Conf. Lisabon, 2000, Soringer verl.,Berlin, 201, p. 1046.
- [44] S. Furihata *et al.*, JAERI Data Code 2002-015 Report.
- [45] W. Friedman and W. Lynch, Phys. Rev. **C 28**, 16 (1983).
- [46] W. Myers and W. Swiatecki, Phys. Rev. **C 60**, 014606 (1999).
- [47] P. Fong, Phys. Rev. **102**, 436 (1956).
- [48] J. Weber *et al.*, Phys. Rev. **C 13**, 2413 (1976).
- [49] G. Kudyaev *et al.*, Yad. Fiz. **45**, 1534 (1987).
- [50] G. Kudyaev *et al.*, Yad. Fiz. **47**, 1540 (1988).
- [51] B. Wilkins *et al.*, Phys. Rev. **C 14**, 1832 (1976).
- [52] T. Enqvist *et al.*, Nucl. Phys. **A686**, 481 (2001).
- [53] L. Audouin *et al.*, Nucl. Phys. **A768**, 1 (2006).
- [54] J. Taieb *et al.*, Nucl. Phys. **A724**, 413 (2003).
- [55] M. Bernas *et al.*, Nucl. Phys. **A765**, 197 (2006).
- [56] M. Bernas *et al.*, Nucl. Phys. **A725**, 213 (2003).
- [57] M. V. Ricciardi *et al.*, Phys. Rev. **C 73**, 014607 (2006).
- [58] P. Napolitani *et al.*, Phys. Rev. **C 70**, 054607 (2004).
- [59] Y. Titarenko *et al.*, Nucl. Instr. Meth. Phys. Res. **A562**, 801 (2006).
- [60] M. Meier *et al.*, Nucl. Sci. Eng. **110**, 289 (1993).
- [61] S. Leray *et al.*, Phys. Rev. **C 65**, 044621 (2002).